Nonlinear compositional convection in mushy layers

D. N. Riahi
Department of theoretical and Applied Mechanics
216 Talbot Laboratory, 104 South Wright Street
University of Illinois at Urbana-Champaign
Urbana, IL 61801, USA

Abstract

This paper presents some extensions of two main problems of nonlinear compositional convection in horizontal mushy layers during the solidification of binary alloys that were recently investigated by the author (Riahi2002, 2004). Under a near-eutectic approximation and the limit of large far-field temperature, we determine a number of two- and three-dimensional weakly nonlinear solutions, and the stability of these solutions with respect to arbitrary three-dimensional disturbances is then investigated. First, the problem of the oscillatory modes of convection, which was investigated recently in the absence of the main permeability parameter K_1 (Riahi2002), is extended to include the effects of K_1, over a range of values of the other parameters, for both two- and three-dimensional motion. It was found, in particular, that the results reported in Riahi (2002) are recovered if K_1 is zero or sufficiently small. In such case two-dimensional solutions in the form of simple-travelling rolls are mostly the only stable and preferred solutions. However, as in the more realistic cases, if K_1 is not sufficiently small, then such solutions are replaced by preferred and stable three-dimensional solutions, which are mostly simple travelling waves in the form of rectangles, squares or hexagons. Next, we revisit the problem of mixed oscillatory and steady modes of convection (Riahi2004), where some results appeared to be sensitive with respect to the approximated value 3.14 of π used in the numerical calculation. Here we find some updated results, which are based on a more accurate value of 3.141592654 for π, plus some additional new results. In particular, we find a preferred and stable mixed standing and steady modes of hexagonal solution over a relatively wide range of the parameter values whose properties are now appeared to be in much better agreement with the available experimental results (Tait et al.1992).

1. Introduction

Recently Riahi (2002), hereafter referred to as R02, extended the linear work by Anderson and Worster (1996) to some extend by studying the problem of nonlinear compositional convection in horizontal mushy layers during the solidification of binary alloys. He analyzed the oscillatory modes of convection in particular range of the parameter values where the critical value $R_c^{(o)}$ of the scaled Rayleigh number R for the

onset of oscillatory convection is distinctly lower than the critical value $R_c^{(s)}$ of R for the onset of steady convection. His results indicated preference of supercritical simple travelling rolls over most of the studied range of the parameter values, while supercritical standing rolls could be preferred only over a rather small range of the parameter values. His detailed nonlinear study of the oscillatory modes of convection in mushy layers complemented to some extent the previous nonlinear studies of the stationary convection in mushy layers (Amberg and Homsy1993; Anderson and Worster1995). However, due to the complexity of the oscillatory problem, R02 considered a simplifying assumption by assuming that the main permeability problem K_1 is of order the perturbation amplitude ε ($\varepsilon<<1$). As a result of this restriction, the effects of K_1 did not enter the weakly nonlinear results reported in R02.

More recently Riahi (2004), hereafter referred to as R04, considered a particular range of parameters for nonlinear convection in horizontal mushy layers where $R_c^{(o)}$ and $R_c^{(s)}$ were close to each other, and he developed and analyzed a nonlinear theory in such a parameter regime which takes into account those mixed oscillatory and steady modes of convection with common wave number vectors. The motivation and justification for the that investigation was due to the realization that, under the already established relevant scaling (Anderson and Worster1995, 1996), the linear system of the problem in particular range of the parameter values exhibits both oscillatory and steady modes of convection at very close values of $R_c^{(o)}$ and $R_c^{(s)}$. Such particular range of the parameter values turned out to be of order to that of the available experimental results (Tait et al.1992). Hence, to determine the analytical results, which could be applicable to such range of the parameter values and, in particular, could be compared with the available experimental results (Tait et al.1992) with some confidence, such a nonlinear theory for the mixed modes of oscillatory and steady convection was needed to be developed and analyzed.

In R02 and R04 analytical expressions for the weakly nonlinear solutions to the problem together with their stability, using perturbation and stability analysis, were determined, and the results were calculated from those analytical expressions, which involved π number, and using the value 3.14 forπ. However, very recently it was found that more exact value of π will be needed to provide with more accuracy the details of some results, which correspond to a small range of values of the linear frequency in a small but particular range of values for a composite parameter G_t, to be defined later in the section 3. A short note that calculates the results based on a more exact value of π and provides the details of those results, which depended significantly on more exact value of π, was already added online to the supplementary materials for R02 since the main qualitative results reported in R02 remained unchanged. However, in regard to the results reported in R04, some of those results and specially the stability results at local values of the *parameters* were depended sensitively on the accurate value of π and providing a note for the results and the associated figures, based on the sufficiently accurate value of π, as a supplemental material online for the later paper was found to be not appropriate.

In the present paper we first extend the work in R02 by including the important effects of K_1 in the analysis and found interesting results. In particular, we found that in

contrast to the results reported in R02, which were effectively valid for zero value of K_1, and depending on the parameter values three-dimensional supercritical solutions in the form of oscillatory rectangles, squares or hexagons can be the preferred and stable form of the compositional convection in a mushy layer. We also calculated the results for the mixed mode cases (R04) based on the sufficiently accurate value of π. We report here some new results not reported in R02, such as those for the nonlinear frequency ω_{11}, and some updated figures and results calculated based on the sufficiently accurate π-value of those already reported in R04 for π=3.14. We find some interesting results. In particular, we find that the preferred mixed solution in the form of standing hexagons-steady hexagons has now much better agreement with the available experimental results (Tait et al.1992) than the one reported in R04 based on the calculation with π=3.14.

The preferred solutions that we referred to earlier in the previous paragraphs, were based on the assumption of the type adopted before by Busse (1975) that the solution, which exists at the lowest value of the control parameter R, is the physically preferred solution. This assumption can follow from the stability results (Busse1967; Riahi1983). In the present paper we follow Busse (1975) and, in addition, carry out stability analysis of the finite-amplitude solutions to determine the preferred and stable solutions.

The following two sections 2-3 deal with the governing system and the finite-amplitude and stability analyses. The results and discussion for the solutions and stability of the oscillatory and mixed modes are presented, respectively in sections 4 and 5, which are followed by conclusion in section 6.

2. Governing system

We consider a binary alloy melt that is cooled from below and is solidified at a constant speed V_0. Following Amberg and Homsy (1993) and Anderson and Worster (1995), we consider a horizontal mushy layer of thickness d adjacent and above the solidification front to be physically isolated from the overlying liquid and underlying solid zones. The overlying liquid is assumed to have a composition $C_0 > C_e$ and temperature $T_\infty > T_L(C_0)$ far above the mushy layer, where C_e is the eutectic composition, $T_L(\tilde{C})$ is the liquidus temperature of the alloy and $\tilde{C}$ is the composition. It is then assumed that the horizontal mushy layer is bounded from above and below by rigid and isothermal boundaries. We consider the solidification system in a moving frame of reference $o\tilde{x}\tilde{y}\tilde{z}$, whose origin lies on the solidification front and translating at the speed V_0 with the solidification front in the positive $\tilde{z}$-direction. The reader is referred to R02 for the motivation and justification in using the Amberg and Homsy (1993) type of model for the present study.

The equations for Darcy-momentum, continuity, heat and solute for the flow in the mushy layer in the already described moving frame are non-dimensionalized by using V_0, k/V_0, k/V_0^2, $\beta\Delta C\rho g k/V_0$, ΔC and ΔT as scales for velocity, length, time, pressure,

solute and temperature, respectively. Here k is the thermal diffusivity, ρ is a reference (constant) density, $\beta=\beta^*-\Gamma\alpha^*$, where α^* and β^* are the expansion coefficients for the heat and solute, respectively, and Γ is the slope of the liquidus, which is assumed to be a constant, $\Delta C=C_0-C_e$, $\Delta T=T_L(C_0)-T_e$ and T_e is the eutectic temperature. The non-dimensional form of the equations for Darcy-momentum, continuity, temperature and solute concentration in the mushy layer are then

$$K(\tilde{\phi})\,\tilde{\boldsymbol{u}} = -\nabla\tilde{P}-\tilde{R}\tilde{\theta}\boldsymbol{z}, \tag{1a}$$

$$\nabla.\tilde{\boldsymbol{u}}=0, \tag{1b}$$

$$(\partial/\partial\tilde{t}-\partial/\partial\tilde{z})(\tilde{\theta}-S_t\,\tilde{\phi})+\tilde{\boldsymbol{u}}.\nabla\tilde{\theta}=\nabla^2\,\tilde{\theta}, \tag{1c}$$

$$(\partial/\partial\,\tilde{t}-\partial/\partial\,\tilde{z})[(1-\tilde{\phi})\tilde{\theta}+C_r\,\tilde{\phi}]+\tilde{\boldsymbol{u}}.\nabla\tilde{\theta}=0, \tag{1d}$$

where $\tilde{\boldsymbol{u}}=\tilde{u}\boldsymbol{x}+\tilde{v}\boldsymbol{y}+\tilde{w}\boldsymbol{z}$ is the volume flux per unit area, $\tilde{u}$ and $\tilde{v}$ are the horizontal components of $\tilde{\boldsymbol{u}}$ in the $\tilde{x}$– and $\tilde{y}$-directions, respectively, $\boldsymbol{x}$ and $\boldsymbol{y}$ are unit vectors in the positive $\tilde{x}$- and $\tilde{y}$-directions, $\tilde{w}$ is the vertical component of $\tilde{\boldsymbol{u}}$ in the $\tilde{z}$-direction, $\boldsymbol{z}$ is a unit vector in the positive $\tilde{z}$-direction, $\tilde{P}$ is the modified pressure, $\tilde{\theta}$ is the non-dimensional form of either composition or temperature as shown in R02, $\tilde{t}$ is the time variable, $\tilde{\phi}$ is the local solid fraction, $\tilde{R}=\beta\Delta C g\Pi(0)/(V_0\nu)$ is the Rayleigh number, $\Pi(0)$ is reference value at $\tilde{\phi}=0$ of the permeability $\Pi(\tilde{\phi})$ of the porous medium, ν is the kinematic viscosity, g is acceleration due to gravity, $K(\tilde{\phi})\equiv\Pi(0)/\Pi(\tilde{\phi})$, $S_t=L/(C_L\,\Delta T)$ is the Stefan number, C_L is the specific heat per unit volume, L is the latent heat of solidification per unit volume, $C_r=(C_s-C_0)/\Delta C$ is a concentration ratio, and C_s is the composition of the solid-phase forming the dendrites. Equation (1d) is based on the limit of sufficiently large value of the Lewis number k/k_s, where k_s is the solute diffusivity. The above equations are subject to the following boundary conditions:

$$\tilde{\theta}+1=\tilde{w}=0 \quad \text{at} \quad \tilde{z}=0, \tag{1e}$$

$$\tilde{\theta}=\tilde{w}=\tilde{\phi}=0 \quad \text{at} \quad \tilde{z}=\delta, \tag{1f}$$

where $\delta=dV_0/k$ is a growth Peclet number representing the dimensionless depth of the layer.

Next, we consider the following rescaling in the limit of sufficiently small δ:

$$C_r=C/\delta,\ S_t=S/\delta,\ \varepsilon<<\delta<<1, \tag{2a}$$

$$(\tilde{x},\tilde{y},\tilde{z})=\delta(x,y,z),\ \tilde{t}=\delta^2 t,\ R^2=\delta\tilde{R}, \tag{2b}$$

$$(\tilde{\theta},\tilde{\phi},\tilde{\boldsymbol{u}},\tilde{P})=(\theta_B,\phi_B,0,P_B)+\varepsilon[\theta(x,y,z,t),\phi(x,y,z,t),(R/\delta)\boldsymbol{u}(x,y,z,t),RP(x,y,z,t)], \tag{2c}$$

where C and S are order-one quantities as $\delta\to 0$, ε is small perturbation amplitude, and the quantities with subscript 'B' are the basic flow variables for the motionless state, which are a function of z only and are given below in terms of asymptotic expansions for small δ

$$\theta_B = (z-1)+\delta(z-z^2)G/2+..., \tag{3a}$$

$$\phi_B = \delta(1-z)/C+\delta^2[-(1-z)^2/C^2+(z^2-z)G/(2C)]+..., \tag{3b}$$

$$P_B = P_0+R[(z-z^2/2)+\delta(z^2/2-z^3/3)G/2+...], \tag{3c}$$

where $G \equiv 1+S/C$ and P_0 is a constant. Since ϕ is small, the following expansion for $K(\tilde{\phi})$ is considered

$$K(\tilde{\phi}) = 1+K_1\tilde{\phi}+K_2\tilde{\phi}^2+..., \tag{4}$$

where K_1 and K_2 are constants.

For the analysis presented in the next section, it was found to be convenient to use the general representation

$$\boldsymbol{u} = \boldsymbol{\Omega} V+\boldsymbol{E}\Psi,\ \boldsymbol{\Omega}\equiv\nabla\times\nabla\times\boldsymbol{z},\ \boldsymbol{E}\equiv\nabla\times\boldsymbol{z}, \tag{5}$$

for the divergent-free vector field $\boldsymbol{u}$ (Chandrasekhar1961), where V and Ψ are the poloidal and toroidal functions for $\boldsymbol{u}$, respectively. By taking the vertical component of the curl of (1a), it can be shown that the toroidal part $\boldsymbol{E}\Psi$ of $\boldsymbol{u}$ must vanish. Taking the vertical component of the double curl of (1a) and using (1b) and (5) in (1), we find the final version of the governing system

$$\nabla^2[K(\phi_B+\varepsilon\phi)\Delta_2 V]+(\partial/\partial z)[\boldsymbol{\Omega}V.\nabla K(\phi_B+\varepsilon\phi)]-R\Delta_2\theta = 0, \tag{6a}$$

$$(\partial/\partial t-\delta\partial/\partial z)(-\theta+S\phi/\delta)+R\,(\mathrm{d}\theta_B/\mathrm{d}z)\Delta_2 V+\nabla^2\theta = \varepsilon R\boldsymbol{\Omega}\mathrm{V}.\nabla\theta, \tag{6b}$$

$$(\partial/\partial t-\delta\partial/\partial z)[(-1+\phi_B)\theta+\theta_B\phi+\varepsilon\phi\theta-C\phi/\delta]+R\,(\mathrm{d}\theta_B/\mathrm{d}z)\Delta_2 V = \varepsilon R\boldsymbol{\Omega}V.\nabla\theta, \tag{6c}$$

$$\theta = V = 0 \qquad \text{at} \qquad z=0, \tag{6d}$$

$$\theta = V = \phi = 0 \qquad \text{at} \qquad z=1, \tag{6e}$$

where

$$\Delta_2 \equiv \partial^2/\partial x^2+\partial^2/\partial y^2.$$

3. Analysis

Similar to the analyses presented in R02 and R04, we first carry out a weakly nonlinear analysis, based on a double-series expansions in powers of δ and ε, to determine the finite-amplitude oscillatory and mixed solutions and then investigate the stability of such solutions. Because of the similarity of the present analysis with the corresponding ones in R02 and R04, we make the description of the analysis here as short as possible and at the same time make the presentation somewhat self-explanatory to the reader. As in the finite-amplitude analysis carried out in R02, we first make a formal asymptotic expansion in ε and then at each order in ε make a formal asymptotic expansion in δ. Since we investigate both steady and oscillatory modes of convection, the following expansions are for the dependent variables of the perturbation system (1), R and the frequency ω for the oscillatory modes of convection:

$$(V, \theta, \phi, R, \omega)=[(V_{00}+\delta V_{01}+....), (\theta_{00}+\delta\theta_{01}+....), (\phi_{00}+\delta\phi_{01}+....), (R_{00}+\delta R_{01}+....),$$

$$(\omega_{00}+\delta\omega_{01}+....)]+\varepsilon[(V_{10}+\delta V_{11}+....), (\theta_{10}+\delta\theta_{11}+....), (\phi_{10}+\delta\phi_{11}+....), (R_{10}+\delta R_{11}+....), (\omega_{10}$$

$$+\delta\omega_{11}+....)]+ \varepsilon^2[(V_{20}+\delta V_{21}+...), (\theta_{20}+\delta\theta_{21}+...), (\phi_{2(-1)} /\delta+\phi_{20}+\delta\phi_{21}+...), (R_{20}+\delta R_{21}+...), (\omega_{20}$$

$$+\delta\omega_{21}+...)]+.... \qquad (7)$$

The analyses for the oscillatory and mixed modes were already done in R02 and R04, respectively. Hence, no details will be provided here and, instead, the main procedure and results of the analysis are given briefly for the oscillatory and steady modes, where the wave number vectors of the oscillatory modes are assumed to be those of the mixed modes.

We consider first the oscillatory modes for the linear problem. At order $1/\delta$ we find $\omega_{00}=0$. At order δ^0 we find

$$V_{00}^{(o)} =\{[\pi^2+(a^{(o)})^2]/[R_{00}^{(o)}(a^{(o)})^2 G]\}\sin(\pi z)\sum_{m=-N}^{N} (A_m^{+}\eta_m^{+}+ A_m^{-}\eta_m^{-}), \qquad (8a)$$

$$\theta_{00}^{(o)} = - \sin(\pi z)\sum_{m=-N}^{N} (A_m^{+}\eta_m^{+}+ A_m^{-}\eta_m^{-}), \qquad (8b)$$

$$\phi_{00}^{(o)} =\sum_{m=-N}^{N} [f_m(z)A_m^{+}\eta_m^{+}+ f_m^{*}(z)A_m^{-}\eta_m^{-}], \qquad (8c)$$

where

$$\eta_m^{\pm} \equiv exp[i(\boldsymbol{a}_m.\boldsymbol{r} \pm S_m\omega_{01}t)], \qquad (8d)$$

$$R_{00}^{(o)} =[(\pi^2+a^2)^2/(a^2 G]]^{0.5}, \qquad (8e)$$

$$f_m(z)=\{- 2\pi^3/[CG(\pi^2 -\omega_{01}^2)]\}\{i\,\omega_{01}S_m/\pi)\sin(\pi z)+\cos(\pi z)+\exp[i\,\omega_{01}S_m(z-1)]\} \qquad (8f)$$

and

$$S_m=1 \text{ for } m>0 \text{ and } -1 \text{ for } m<0. \tag{8g}$$

Here the quantities with a superscript 'o' represent those for the oscillatory modes, i is the pure imaginary number ($i\equiv\sqrt{-1}$), subscript 'm' takes only non-zero integer values from $-N$ to N, N is a positive integer, $\boldsymbol{r}$ is the position vector, and the horizontal wave number vectors $\boldsymbol{a}_m$ satisfy the properties

$$\boldsymbol{a}_m \cdot \boldsymbol{z} =0,\ |\boldsymbol{a}_m|=a,\ \boldsymbol{a}_{-m}=-\boldsymbol{a}_m. \tag{9}$$

The coefficients A_m^+ and A_m^- satisfy the conditions

$$\sum_{m=-N}^{N}(|A_m^+|^2+|A_m^-|^2)=2,\ A_m^{\pm *}=A_{-m}^{\pm}, \tag{10}$$

where the asterisk indicates the complex conjugate. Minimizing the expression for $R_{00}^{(o)}$, given in (5d), with respect to the wave number a, we find

$$R_{00c}^{(o)}=2\pi/\sqrt{G},\ a_c=\pi. \tag{11}$$

We now consider the steady modes for the linear problem. At the lowest order δ^0 we find

$$V_{00}^{(s)}=[1/(\pi\sqrt{G})]\sin(\pi z)\sum_{n=-N}^{N}(A_n\,\eta_n), \tag{12a}$$

$$\theta_{00}^{(s)}=-\sin(\pi z)\sum_{n=-N}^{N}(A_n\eta_n), \tag{12b}$$

$$\phi_{00}^{(s)}=[-2\pi/(CG)][1+\cos(\pi z)]\sum_{n=-N}^{N}(A_n\eta_n), \tag{12c}$$

$$R_{00}^{(s)}=[(\pi^2+a^2)^2/(a^2G)]^{0.5}, \tag{12d}$$

where

$$\eta_n\equiv exp(i\boldsymbol{a}_n.\boldsymbol{r}). \tag{12e}$$

Here the quantities with a superscript 's' represent those for the stationary modes, subscript 'n' takes only non-zero integer values from $-N$ to N, N is a positive integer, and the coefficients A_n satisfy the conditions

$$\sum_{n=-N}^{N}|A_n|^2=1,\ A_n^*=A_{-n}. \tag{13}$$

Minimizing the expression for $R_{00}^{(s)}$, given in (9d), with respect to the wave number a, we find the same results as in the case of the oscillatory modes, which are given in (11).

It turns out that for all the values of the parameters where the oscillatory modes exist based on the present formulation, the critical values $R_c^{(o)}$ and $R_c^{(s)}$ of R at the onset of motion for the oscillatory and steady modes, respectively, which were derived in R04

using (11) and the solvability conditions at order δ for the oscillatory and steady systems, always satisfy the condition

$$R_c^{(o)} < R_c^{(s)}, \tag{14}$$

and the difference $(R_c^{(s)}-R_c^{(o)})$ is small and decreases with decreasing $G_t \equiv (G\text{-}1)/(CG^2)$. The minimum value of G_t for which oscillatory mode exist, is 0.5 (Anderson and Worster1995). Hence, in the limit of sufficiently small G_t, we superimpose the steady solution on the most critical oscillatory solution in the order δ^0, which yield the following mixed solution

$$(V_{00}, \theta_{00}, \phi_{00}) = [V_{00}^{(o)}, \theta_{00}^{(o)}, \phi_{00}^{(o)}] + B[V_{00}^{(s)}, \theta_{00}^{(s)}, \phi_{00}^{(s)}], \tag{15}$$

where B is an arbitrary constant. To investigate the convection due to oscillatory modes alone, we set $B \equiv 0$ in (17).

Next, the nonlinear problem for the governing system (6) at order ε is analyzed. At order ε/δ, we find $\omega_{10} = 0$. At order ε the system (6a)-(6e) can be reduced to the form given by (A1) in the Appendix for the oscillatory convection case and by (A1) in R04 for the mixed convection case. Following the same reasoning given in R02, the solvability conditions for the nonlinear system (A1) for oscillatory case yield $R_{10}=0$, while those for the system at order εδ also yield $R_{11} = \omega_{10}=0$. The solvability conditions for the mixed system at order ε yield two sets of equations, which are reduced to those given by (A2a) and (A2b) in R04. In these equations an angular bracket indicates the average over the layer. There are two major new of mixed solutions for which R_{10} is non-zero and can represent one class of subcritical convection cases, where $\varepsilon R_{10} < 0$, and one class of supercritical convection cases, where $\varepsilon R_{10} > 0$.

The types of solutions that can be realized or be preferred by the nonlinear system are described here briefly as follows. The simple traveling form of oscillatory solutions or component of the mixed solutions can be in the form of either right-travelling mode, where the phase velocity of the mode is in the direction of the component of the mode's wave vector along ***r***, or in the form of left-travelling mode where the phase velocity of the mode is in the direction opposite to that of the component of the mode's wave vector along ***r***. Since identical nonlinear results are obtained for either left- or right-travelling modes, the analysis in this paper for the case of simple traveling modes is presented only in the form of right-travelling modes. For the right-travelling-steady mixed solutions in the so-called 'semi-regular' case, in which scalar product between any one of the ***a***-vectors and its two neighbouring ***a***-vectors assumes the constant values α_1 and α_2 (Busse 1967; R02), we have

$$|A_1^+| = \ldots = |A_N^+| = 0, \; |A_1^-|^2 = \ldots = |A_N^-|^2 = 1/N, \tag{16a}$$

and

$$|A_1|^2 = \ldots = |A_N|^2 = 1/(2N), \tag{16b}$$

while only (16a) holds for case of right-travelling form of the oscillatory solutions. For the case of regular solutions, we have $\alpha_1 = \alpha_2$. For the oscillatory solutions or component of the mixed solutions in the form of standing waves, we have $A_n^+ = A_n^-$ for every n. For the standing wave-steady mixed solutions, we have (16b) and

$$|A_1^{\pm}|^2 = \ldots = |A_N^{\pm}|^2 = 1/(2N), \tag{16c}$$

while only (16c) holds for the oscillatory solutions in the form of standing waves. For the oscillatory solutions or component of the mixed solutions in the form of general travelling waves of the types introduced in R02 and in the semi-regular case, we have (16b) and

$$A_1^+ = \ldots = A_N^+ = [(0.5\text{-b})/N]^{0.5},\ A_1^- = \ldots = A_N^- = [(0.5+\text{b})/N]^{0.5}, \tag{16d}$$

while only (16d) holds for the semi-regular oscillatory solutions in the form of general traveling waves. The constant b in (16d), which is restricted in the range

$$|\text{b}| < 0.5 \tag{16d}$$

(R02), is the parameter for the general traveling wave, whose specific value in the range (16d) provides particular general travelling wave solutions or component of the mixed solutions. As explained in R04, the coefficient R_{10} is non-zero only for the solutions in the form of hexagons. The mixed hexagonal solutions with the oscillatory components in the form of simple-travelling wave, standing wave and general-travelling wave were called in R04 as solutions numbers 1, 2 and 3, respectively.

The system of equations and boundary conditions at order ε are already given in R04 for the mixed case and by (A1) in the Appendix for the oscillatory case. The expressions for the solutions V_{10}, θ_{10} and ϕ_{10} of this system, which will be needed for the analysis of the governing system at $O(\varepsilon^2)$, are given in the supplement to the online version of R04 for the mixed case, and they are given below for the oscillatory case

$$(V_{10}, \theta_{10}) = \sum_{l,p=-N}^{N} [(B_{lp}^{(o)}, E_{lp}^{(o)})(A_l^+ A_p^+ \eta_l^+ \eta_p^+ + A_l^- A_p^+ \eta_l^- \eta_p^+) + (B_{lp}^{(o)*}, E_{lp}^{(o)*})(A_l^+ A_p^- \eta_l^+ \eta_p^- + A_l^- A_p^- \eta_l^- \eta_p^-)], \tag{17a}$$

$$\phi_{10} = \sum_{l,p=-N}^{N} [f_{lp}^{(11)} A_l^+ A_p^+ \eta_l^+ \eta_p^+ + f_{lp}^{(12)} A_l^+ A_p^- \eta_l^+ \eta_p^- + f_{lp}^{(21)} A_l^- A_p^+ \eta_l^- \eta_p^+ + f_{lp}^{(22)} A_l^- A_p^- \eta_l^- \eta_p^-] + \sum_{m=-N}^{N} (f_m^+ A_m^+ \eta_m^+ + f_m^- A_m^- \eta_m^- + g_m^+ A_m^+ \eta_m^+ + g_m^- A_m^- \eta_m^-), \tag{17b}$$

where the expressions for the coefficients $B_{lp}^{(o)}$, $E_{lp}^{(o)}$, $f_{lp}^{(ij)}(i,j=0, 1, 2)$, f_m^+, f_m^-, g_m^+ and g_m^-, which are generally functions of z, are given by (A3) and (A4) in the Appendix.

The solvability conditions for the system at order ε^2/δ yield $\omega_{20}=0$ and trivial (zero) solutions follow for the dependent variables. At order ε^2 the system (6a)-(6e) can

be reduced to the form given in R04 for the mixed case, and for the oscillatory case they are reduced to the form given by (A4) in the Appendix. The solvability conditions for this system yield to a system of equations, which are given in R04 for the mixed case, and for the oscillatory case is the one given by (A9) in the Appendix. The system (A9) for the oscillatory case contain integral expressions of the form $<\eta_n^{\pm}\,\eta_m^{\pm}\,\eta_l^{\pm}\,\eta_p^{\pm}>$, which differ from zero only if

$$\boldsymbol{a}_n+\boldsymbol{a}_m+\boldsymbol{a}_l+\boldsymbol{a}_p=0 \tag{18a}$$

and

$$\pm S_n\pm S_m\pm S_l\pm S_p=0 \tag{18b}$$

hold. Using the conditions (18a)-(18b) in (A9), we find the following simplified equations:

$$R_{20}\sqrt{G}\,\pi(|A_n^{+}|^2+|A_n^{-}|^2)=\sum_{m=-N}^{N}\{[T_{nm}^{(o1)}|A_n^{+}|^2|A_m^{+}|^2+T_{nm}^{(o2)}A_n^{-}A_m^{-}A_{-n}^{+}A_{-m}^{+}\,\delta(S_n+S_m)+$$

$$T_{nm}^{(o3)}|A_n^{-}|^2|A_m^{+}|^2+T_{nm}^{(o4)}A_n^{+}A_m^{-}A_{-n}^{-}A_{-m}^{+}\delta(S_n-S_m)+T_{nm}^{(o5)}A_n^{-}A_m^{+}A_{-n}^{+}A_{-m}^{-}\delta(S_m-S_n)+T_{nm}^{(o6)}$$

$$|A_n^{+}|^2|A_m^{-}|^2+T_{nm}^{(o7)}A_n^{+}A_m^{+}A_{-n}^{-}A_{-m}^{-}\delta(S_n+S_m)+T_{nm}^{(o8)}|A_n^{-}|^2|A_m^{-}|^2]\},$$

$$(n=-N, ..., -1, 1, ..., N), \tag{19a}$$

where

$$\delta(a)=1 \text{ for } a=0 \text{ and } 0 \text{ for } a\neq 0, \tag{19b}$$

and the expressions for $T_{nm}^{(oi)}$(i=1, ..., 8) are given, respectively, by (A6a)-(A6h) in the Appendix. The expressions for $T_{nm}^{(oi)}$ turn out to satisfy the symmetry conditions of the form

$$T_{nm}^{(oi)}=T_{mn}^{(oi)}\ (i=1, ..., 8). \tag{19c}$$

Since the simplest types of solutions are often observed in the applications, we restrict our attention to the simplest types of oscillatory or mixed solutions, which are either regular or semi-regular. As presented in R04, for the mixed case the solvability conditions at order ε^2 provide equations, which, in particular, contain R_{20} and ω_{11}, where the nonlinear frequency ω_{11} turns out to be non-zero only for the mixed solutions in the form of hexagons (R04). Simple form of regular and mixed types of solutions correspond to the cases of two-dimensional oscillatory rolls-steady rolls (N=1), oscillatory squares-steady squares (N=2) and oscillatory hexagons-steady hexagons (N=3), while those for a semi-regular and mixed types of solution correspond to the cases with different values of angle γ of oscillatory rectangles-steady rectangles (N=2). Here, γ ($0<\gamma<90°$) or $180°-\gamma$ is the angle between any two adjacent wave number vectors of a

rectangular cell for a particular solution in the form of rectangles. Likewise, simple forms of regular and semi-regular oscillatory types of solutions correspond to rolls, squares, rectangles and hexagons. In R04 the mixed solutions with the oscillatory components in the forms of simple-travelling rolls, standing rolls, general-travelling rolls, simple-traveling rectangles, standing rectangles, general-travelling rectangles, simple-travelling squares, standing squares and general-travelling squares are designated as solutions 4, 5, 6, 7, 8, 9, 10, 11 and 12, respectively.

To distinguish the physically realizable finite-amplitude solutions among all the possible oscillatory or mixed solutions, the stability of V, θ, ϕ with respect to arbitrary three-dimensional disturbances V_d, θ_d, ϕ_d is investigated. The time-dependent disturbances can be assumed in the form

$$(V_d,\theta_d,\phi_d)=[V'(x, y, z, t), \theta'(x, y, z, t), \phi'(x, y, z, t)]exp(\sigma t), \tag{20}$$

where σ is the growth rate of the disturbances. When the governing equations and the boundary conditions of the form (6a)-(6e) for the finite-amplitude flow are subtracted from the corresponding equations and boundary conditions for the total dependent variables for the finite-amplitude flow and the disturbance quantities, and the resulting system is linearized with respect to the disturbance quantities, we obtain the stability system, which is given by (A7a)-(A7e) in Appendix.

When the expansion (7) is used in (A7a)-(A7e), it becomes evident that the stability system can be solved by a similar expansion

$$\begin{aligned}(V', \theta', \phi', \omega', \sigma)=&[(V'_{00}+\delta V'_{01}+...), (\theta'_{00}+\delta\theta'_{01}+...), (\phi'_{00}+\delta\phi'_{01}+...), (\omega'_{00}+\delta\omega'_{01}+...),\\ &(\sigma_{00}+\delta\sigma_{01}+...)]+\varepsilon[(V'_{10} +\delta V'_{11}+...), (\theta'_{10}+\delta\theta'_{11}+...), (\phi'_{10}+\delta\phi'_{11}+...), (\omega'_{10}+\delta\omega'_{11}+...),\\ &(\sigma_{10}+\delta\sigma_{11}+...)]+\varepsilon^2[(V'_{20}+\delta V'_{21}+...), (\theta'_{20}+ \delta\theta'_{21}+...), (\phi'_{2(-1)}/\delta+\phi'_{20}+\delta\phi'_{21}+...), (\omega'_{20}+\delta\omega'_{21}\\ &+...), (\sigma_{20}+\delta\sigma_{21}+...)]+...,\end{aligned} \tag{21}$$

where the expansion for ϕ' is singular at order ε^2 as $\delta\to 0$, but again as in the cases in R02 and R04, the $O(1/\delta)$ term is needed in the stability analysis since the $O(\varepsilon^2)$ stability problem is found to be forced by a term of order $1/\delta$ in the solute equation for the disturbances. Following the assumptions and procedures described in R02 for the oscillatory disturbances and in R04 for the mixed disturbances, we find the most critical disturbances, which have the maximum growth rate, are characterized by $\sigma_0=0$, where

$$\sigma_0=\sigma_{00}+\delta\sigma_{01}+...$$

Then the linear and nonlinear solutions for the dependent variables of the disturbances at order δ^0 and ε are found, where the lengthy solvability conditions for the disturbance system at order ε determines σ_{10} for the mixed case, which is discussed in R04, and for the oscillatory case, the analysis similar to that in R03 yield $\sigma_{10}=0$. Next, we applied the very lengthy solvability conditions for (A7a)-(A7e) at order ε^2 , which will not be given here, to determine σ_{20}. The leading order growth rate $\sigma^*=\varepsilon\sigma_{10}+\varepsilon^2\sigma_{20}$ of the disturbances

acting on the finite-amplitude oscillatory or mixed motion can then be determined from these systems following the method of approach due to Busse (1967), which is now a standard stability procedure.

4. Results and discussion for oscillatory case

4.1. Linear problem

The linear system with its eigenvalue problem for oscillatory and modes, which led to the results (8)-(11), are in general, functions of the physical parameters C, S and K_1. Although the scaled Stefan number S and the scaled compositional ratio C were represented earlier partly in terms of the composite parameters G and G_t for the simplicity in formulation, we are interested in this section to present and discuss the results for the oscillatory case instead in terms of the already referred physical parameters. It should also be noted that in typical experiments with ammonium chloride-water solutions, like those of Tait et al. (1992), the values of the scaled concentration ratio and the scaled Stefan number are about $C \approx 20\delta$ and $S \approx 5\delta$, so that for a sufficiently thin mushy layer, the results presented in this section, which are for the range of values $0.0355 \leq C \leq 0.2461$ and $S=0.25C$, could at least be qualitatively relevant. The linear results were already presented in Anderson and Worster (1996) and in R02 (see also online supplementary materials to R02) mainly in terms of the composite parameters G and G_t. Here we briefly present the linear results in terms of the physical parameters. The frequency ω_{01} of the oscillatory solutions does not depend on K_1. For $S=0.25C$, ω_{01} increases with C. It has a higher rate of increase with C at higher values of C. The critical value $R_c^{(o)}$ of the scaled Rayleigh number increases with K_1, but it decreases with increasing C. Since S represents a measure of the latent heat relative to the heat content and C represents a measure of the difference between the characteristic compositions of the solid and liquid phases and the compositional variation of the liquid, then the linear system is stabilized as C increases for a given S, or as S decreases, for a given C. Since $S=0.25C$ in the present calculation, the effect of the Stefan number dominates over that of the composition ratio and the flow is destabilizing as C increases. The stabilizing effect on the linear system when K_1 increases, is consistent with the physical role played by K_1 since the permeability of the mushy layer decreases with increasing K_1.

4.2. Nonlinear problem

Important quantity due to the nonlinear oscillatory effects is the coefficients R_{20}, which is calculated in the present study. Since $R_{10}=0$ for the oscillatory case, then it can be seen from the expansions (7) that R_{20} represents leading contributions to the change in R required to obtain finite amplitude ε for a nonlinear solution. In terms of these coefficients the amplitude of convection is of order

$$|\varepsilon| = [(R - R_c^{(o)})/R_{20}]^{0.5}. \tag{22}$$

It should also be noted that for a given value of $R > R_c^{(o)}$, which corresponds to the supercritical convection state, the expression (22) for $|\varepsilon|$ is maximum, among all the

solutions of the nonlinear problem, only if R_{20} has the smallest positive value for particular solution, and in this sense such particular solution is referred to as the preferred solution in this paper. The sign of R_{20} determines whether the oscillatory solution exists for values of R above or below $R_c^{(o)}$. For $R_{20}<0$, which corresponds to the subcritical convection state, $R<R_c$ and $|\varepsilon|$ decreases with increasing R, which corresponds to an unstable state as our stability analysis actually indicated. In the present problem the coefficient R_{20} is due to the nonlinear convective terms in the temperature equation and the nonlinear interactions between the flow velocity and the non-uniform and nonlinear permeability associated with the perturbation to the basic state solid fraction.

Oscillatory hexagons

We begin the presentation of the results and the corresponding discussion for the cases of oscillatory solutions in the form of hexagons because of the available experimental observation of such flow pattern (Tait et al.1992). The coefficient R_{20} for the solutions in the form of simple travelling hexagons, standing hexagons and general travelling hexagons, were computed for S=0.25C and various values of C, K_1 and K_2. The sign of R_{20} determines whether the oscillatory solution exists for values of R above or below $R_c^{(o)}$. Here we are interested to study the preferred oscillatory hexagonal type of solutions, which, as to be presented later in this section, turn out to be stable, for particular range of values of the parameters, and correspond to the relatively lowest values of R. These types of oscillatory solutions should correspond to the smallest values of $R_{20}>0$. We calculated the values of R_{20} for the oscillatory solutions for S=0.25C but for different values of C, K_1 and K_2, where the experimentally relevant range of S and C referred to earlier in this section could be covered. In all the calculations that we carried out, we found that simple-travelling hexagons have mostly smaller values of R_{20} as compared with other types of hexagonal solutions, the value of R_{20} increases with K_2, and the value of positive R_{20} often decreases with increasing K_1 or decreasing C and eventually R_{20} becomes negative. When the coefficient R_{20} just changes sign for particular values of the parameters, there is neighboring points in parameter space where such coefficient is positive but has very small magnitude and, thus, the corresponding solution is often preferred. Our generated data for R_{20} for the above stated three types of solutions and for different parameter values indicate that the effect of K_2 is generally stabilizing in the sense that the value of R_{20} increases with K_2, and its values for the solutions in the form of standing hexagons and general-travelling hexagons only few times, which depend on the parameter values, can become smaller than the one for simple-travelling hexagons, but simple-travelling hexagons are mostly preferred as compared with the later two types of solution especially at lower values K_1. Some typical results about the effects of C and K_1 are presented in Figure 1 for R_{20} of the simple-travelling hexagonal solution for S=0.25C, K_2=0 and for several values of K_1. As can be seen from this figure, there is a sizable in C where the stabilizing effect of C dominates over the destabilizing effect of S, while there is only a small range in C where S dominates over C. The permeability parameter K_1 is destabilizing in the most of the range in C and stabilizing elsewhere.

The present investigation is restricted to the range $K_1<0.1$ and $K_2<0.1$ since for value of each of these parameters beyond this range, the order of magnitude of the

coefficient R_{20} increases rapidly with either K_1 or K_2 becoming much larger than unity by about at least 3 orders of magnitude, so that the modeling assumption of the type (7), which assumes that the coefficients, such as $|R_{20}|$, in those double-expansions in powers of ε and δ be of order unity can no longer be justified.

We also examined the vertical distribution of solid fraction at different time and location in the horizontal direction for the preferred mixed solutions. Our generated data, over most of the periodic domain in time, at centers and at the nodes of the preferred oscillatory solution in the form of preferred hexagons indicated useful information about magnitude and the sign of the perturbation to solid fraction at the nodes and at the centers of the cells. Some typical results are presented in Figures 2 and 3 for the vertical distribution of the basic state (solid line) and total solid fraction at both a center (dashed line) and a node (dotted line) of a preferred standing hexagonal solution. In these calculations δ=0.15, S=0.25C, C=0.1565, K_1=0.085, K_2=0.0, R_{20} =12.46, ω_{01}=5.0 and the value ε is chosen to be the maximum value of $|\varepsilon|$=0.001 beyond which the solid fraction becomes negative. This is based on the physical ground that the value of the perturbation to the solid fraction cannot be such that total solid fraction becomes negative. It is seen from the figure 2, which is drawn at the beginning of the period of oscillation $2\pi/\omega_{01}$, that there is mostly tendency for chimney formation at the node and solid dendrite formation at the center of the cell. Figure 3, which is drawn at a time about half of the period of oscillation later, shows a complete opposite picture to that of the figure 2. That is, the figure 3 shows that there is mostly tendency for channel formation at the center and solid dendrite formation at the node of the same cell. This result may indicate a beneficial effect of the oscillatory mode to at least reduce the tendency for channel formation in the cell. Similar to the discussion provided in R02 for the solid fraction due to the standing modes, the chimneys and the compositional strips are in the vertical direction since the phase speed of these modes is zero, but the vertical extent of the chimneys can vary depending on the variation of the solid-fraction perturbation with respect to time. However, in the case of a traveling wave type of solution, the chimneys and the compositional strips in a travelling wave state can be inclined because of the non-zero values of the phase speed of such a wave relative to the uniform upward speed if the mushy layer (Anderson and Worster 1996; R02).

Oscillatory rolls

Here again R_{20} is the important coefficient for the nonlinear effects for rolls, and the solutions can be in the form of simple travelling rolls, standing rolls or general travelling rolls. The coefficient R_{20} was computed for various values of the parameters. As was the case for all the oscillatory solutions, the effect of K_2 was found to be stabilizing in the sense that R_{20} increases with K_2. The effect of K_1 on R_{20} was found to be mostly stabilizing in the sense that this coefficient mostly increase with increasing K_1. In addition, it was found that the rate of increase of R_{20} with respect to K_2 is much larger than the rate at which R_{20} increases with K_1. For the least stabilizing case where K_2=0, the main results about the coefficient R_{20} are as follows. For not too large value of C the coefficient R_{20} is generally positive and, thus, the flow due to rolls is supercritical. For sufficiently small value of K_1, the preferred solution is that due to simple-travelling rolls. For larger but not too large values of K_1, the value of R_{20} for the simple-travelling rolls is

mostly smaller than those for the standing and general-travelling rolls, but standing rolls can have smaller value of R_{20} as compared with the other two types of rolls if C is sufficiently large. For too large values of K_1, general-travelling rolls have R_{20} mostly smaller than those for the other two types of rolls. For non-zero values of K_2, there is small range for larger values of C where standing rolls are preferred type of solutions if K_1 =0 and are mostly preferred relative to only two other types of rolls in such a range of values for C if K_1 is non-zero and not too small. Some typical results for the oscillatory rolls in the form of simple-travelling, standing and a type of general-travelling waves (b=0.3) are given in Figure 4. It can be seen from this figure that the destabilizing effect of S dominates over the stabilizing effect of C for the lower range of values of C, while the stabilizing effect of C dominates over the destabilizing effect of S for the upper range of values for C. In addition, the simple-travelling rolls are preferred over the other two types of rolls in the lower range of values of C, general-travelling rolls become preferred over the other two rolls-types in a small intermediate range of values of C, and standing rolls are preferred over the other two types of rolls in an upper range of values of C. Comparing values of R_{20} for oscillatory rolls and hexagons for different values of the parameters that we have investigated so far, we find that oscillatory hexagons and particularly simple-travelling hexagons are preferred mostly over the oscillatory rolls if K_1 is not too small. As to be discussed later in this section, all the subcritical mixed solutions with $R_{20}<0$ are found to be unstable and, therefore, such solutions are not preferred.

Oscillatory rectangles

Here we consider oscillatory rectangular solutions, which include those sets of classes of solutions with $\gamma \neq 90°$ and those oscillatory squares with $\gamma=90°$. Again, as in the case of oscillatory rolls and hexagons, the important coefficient for the nonlinear effects is R_{20} for solutions in the form of simple-travelling rectangles, standing rectangles, general- travelling rectangles, simple-travelling squares, standing squares and general-travelling squares. The coefficient R_{20} for these solutions was computed for various values of the parameters. The effect of K_1 on the values of this coefficient for such solutions was found to be non-monotonic in the sense that the effect of this parameter can be either stabilizing or destabilizing depending on the value of K_1, so that the values of this coefficient can increase and then decrease, or vice versa, with increasing K_1. For the least stabilizing case where K_2=0.0, the main results about R_{20} are as follows. The coefficient R_{20} is mostly positive and, thus, the flows due to the rectangular solutions are mostly supercritical. The effect of C on the value of R_{20} is generally non-monotonic in the sense that C has stabilizing or destabilizing effect in different range of values for C. The simple-travelling rectangles are mostly preferred as compared with the other types of oscillatory rectangles. However, for moderate or large values of K_1, there are few cases where either standing rectangles or general-travelling rectangles become preferred relative to other types of the oscillatory rectangles. Some typical results about the dependence of R_{20} for the solutions in the form of simple-travelling squares on C and K_1 are given in Figure 5, where R_{20} is plotted versus C for S=0.25C, K_2=0.0 and for several values of K_1. It can be seen from this figure that the stabilizing effect of C dominates over the destabilizing effect S over most of the investigated range of values of C, except in a small intermediate range of values of C where the destabilizing effect of S dominates

over the stabilizing effect of C. The parameter K_1 is destabilizing over most of the investigated range of values of C, except near the upper range of values of C where K_1 is stabilizing. The range of values in C for which such flow is subcritical is widened with increasing value of K_1.

Figure 6 presents R_{20} of simple-travelling rectangles versus C for S=0.25C, K_1 = 0.045, K_2=0.0 and for three different values of the angle γ. It can be seen from this figure that γ is destabilizing, and the stabilizing effect of C dominates the destabilizing effect of S. Also subcritical domain seems to be diminished with decreasing γ. For the rectangular solution with γ=70°, where a subcritical domain is shown in the figure, there are values in in C at which R_{20} can be sufficiently small and positive leading to the preference of such solution. Comparing the values of R_{20} for the least stable case and for different two- and three-dimensional oscillatory solutions that we investigated so far, we find that over most of the values of the parameters, simple-travelling rectangles and simple-travelling hexagons are mostly preferred over other types of solutions. Some typical results are provided in Figure 7, which presents R_{20} for simple-travelling solutions in the form of rolls, rectangles with γ=70° and hexagons versus C for S=0.25C, K_1=0.025 and K_2=0.0. It can be seen from this figure that hexagons are the preferred pattern over most of the investigated range of values in C, while rectangles replace hexagons only for small intermediate range of values in C or if C is sufficiently small.

4.3. Stability of finite-amplitude oscillatory solutions

Following standard stability procedure (Busse1967), the systems for the growth rate σ^* of the disturbances acting on the finite-amplitude mixed solutions have been simplified, and the expression for σ^* has been computed for different types of solutions. In all the cases that have been investigated only supercritical oscillatory solutions in the form of rolls, rectangles and hexagons are found to be possibly stable in particular range of the values for the non-dimensional parameters.

For sufficiently small K_1, supercritical simple-travelling rolls are stable over most of the domain of the values of C, while supercritical standing rolls are stable over a small domain of relatively large but not too large values of C. The region of stable standing rolls widen somewhat with increasing the values of K_2. For not too small value of K_1 and depending on the values of the parameters, supercritical simple-travelling hexagons or supercritical simple-travelling rectangles can mostly be stable and be preferred over the rest of the detected solutions. There are small regions in the parameter space where other three-dimensional supercritical solutions in the form of standing hexagons, general-travelling hexagons, standing rectangles or general-travelling rectangles can be stable and be preferred over other types of solution. No subcritical solution was found to be stable.

5. Results and discussion for mixed case

In this section we present some new or updated results for the problem studied in R04 for the case where a sufficiently accurate value of π with included 9 decimals (π=

3.141592654) is used in the present numerical calculations of the analytical expression, which were already determined in R04.

The calculated results in R04 were based on the approximate value of $\pi=h\equiv3.14$, where only two digits of the decimals for the value of π were taken into account. However, very recently it was found out that if the more exact value of π such as 3.141592654 is used in the numerical evaluation of the analytical expressions, then the corresponding results remain essentially the same as those for $\pi=h$ everywhere, except in the linear frequency range $2.60<|\omega_{01}|<3.60$. Since the equation for this frequency, which is given by (13b) in R02, has a removable singularity at $|\omega_{01}|=\pi$ and is a function of the composite parameter G_t, the calculated values of G_t, for a given value of the frequency, turns out to become smaller than 0.5 if the approximate value of 3.14 is used for π in the equation for ω_{01} to evaluate numerically the value of G_t for a given value of the frequency. However, if sufficiently exact value of π is used in the calculation, then it is found that the minimum value of G_t for which non-zero ω_{01} exists, is 0.5. Hence, we recalculated the results provided in the section 4 of R04 by using the sufficiently exact value of π in the numerical evaluation of various analytical expressions that were provided in R04. It should be noted that all the materials presented in the abstract, sections 1-3, appendix and reference section of R04 remain totally unchanged and are essentially independent with respect to the above stated accuracy of the value of π used in the numerical evaluations of the analytical expressions. This section provides briefly some updated results and the corresponding figures of those in R04, which were affected by the approximate value of π and, in addition, present some new results that were not reported in R04.

To present the updated and new results, we start from the section 4 in R04 and follow the materials in R04 page by page and we recommend that the reader follows the same section in R04 while reading the present section.

In the sub-section 4.1 of the section 4 in R04 the parts that need to be updated are the appropriate range of values for G_t and the figures 2 and 3. For the present mixed-mode study, we considered the range $0.5002\leq G_t\leq0.534$, which is appropriate for a sufficiently thin mushy layer. Within this range of values for G_t, the critical values $R_c^{(s)}$ and $R_c^{(o)}$ are sufficiently close to one another that makes the mixed-mode analysis quite appropriate. Figures 2 and 3 of R04 are reproduced here for a range slightly larger than this range of values for G_t, and they are labeled figures 8 and 9, respectively. It can be seen from the figure 8 that in contrast to its previous version, the rate of change of the frequency with respect to G_t decreases with increasing G_t. The values of the other parameters used to produce figure 9 are the same as those used before to produce its previous version. For all the values of G_t shown in figure 9, $[R_c^{(s)}-R_c^{(o)}]$ can be considered sufficiently small since its values are less than 1/150 of either $R_c^{(s)}$ or $R_c^{(o)}$.

In the sub-section 4.2 of the section 4 in R04, we start with the nonlinear problem due to oscillatory hexagons-steady hexagons. The few parts that need updating are briefly as follows. The new generated data for R_{10} and R_{20} indicates that the variation of $|R_{10}|$ with respect to G_t is, in general non-monotonic, and R_{20} can become negative for

larger values of K_1. Figure 5 of R04 is reproduced here under the label Figure 10, which presents $R_n \equiv(\varepsilon R_{10} +\varepsilon^2 R_{20})/|\varepsilon|$ versus G_t for subcritical flow in the form of standing down-hexagons-steady down-hexagons with G=1.25, ε=-0.001, K_2=0.0 and for K_1=0.0157, 0.0251 and 0.0314. Although it may be difficult to observe from the figure 10 at low value of K_1, the inspection of the corresponding data indicate that the variation of R_n with respect to G_t is non-monotonic. Using the same solution and the parameter values of figure 10, a new Figure 11 is produced here for the nonlinear frequency ω_{11} versus G_t. As can be seen from this figure, the order of magnitude of the nonlinear frequency can exceed 120. for K_1=0.0314 for lower values of G_t. Since $\omega_{11}<0$ (>0) for $R_{10}>0(<0)$, the nonlinear effect for either standing down-hexagons-steady down-hexagons or standing up-hexagons-steady up-hexagons solutions is to reduce the period of oscillations of such solutions.

The present updated nonlinear investigated was found to be restricted to the range $K_1<0.1$ and $K_2<0.05$ since for values of either of these two parameters beyond its range of values, the magnitude of the coefficient R_{20} increases rapidly with either of these two parameters invalidating the perturbation-modeling assumption of the present study, which assumes that the coefficients, such as $|R_{20}|$, in those double-expansions in powers of ε and δ be of order unity.

Our newly generated data for the vertical distribution of solid fraction for the preferred solution in the form of standing hexagons-steady hexagons in the subcritical down-hexagonal state, indicated that the perturbation to the solid fraction at a node and center of the cells is, respectively, negative and positive over the whole domain of the mushy layer, while for the subcritical up-hexagonal state, the perturbation to the solid fraction at a note and center of the cells is positive and negative, respectively. Typical results are provided in Figures 12 and 13, which reproduce those previous versions presented by the figures 6 and 7 in R04, but here are based on the updated value of G_t=0.502. The values of the other parameters for figures 12 and 13 are the same as those in their previous versions. It can be seen from the figure 12 that there is tendency for channel formation at the node and solid dendrite formation at the center all the way throughout the layer. This result agrees with the available experimental observation (Tait et al.1992) for the down-hexagonal state and is a significant improvement over the corresponding result of the previous version given in R04 where only a partial agreement to the experimental observation was predicted. Figure 13 shows that for up-hexagonal state, there is tendency for solid dendrite formation at the node and channel formation at the center, which contradicts the experimental observation for the channel formation.

Next, we consider the nonlinear problem due to the oscillatory rolls-steady rolls. Our newly generated data in the range $0.5001\leq G_t \leq 0.534$ and for different values of the other parameters for such solutions provided results, which are given briefly as follows. Depending on the values of G_t and K_1, different types of rolls solutions can be preferred relative to other solutions in the forms of rolls. The coefficient R_{20} decreases with increasing K_1. For the least stable case (K_2=0.0), mixed rolls are subcritical for $K_1>0.09$. It should be noted that although steady rolls are found to have smaller R_{20} relative to mixed and oscillatory rolls for $K_1\leq 0.015$, they are not preferred since their critical $R_c^{(s)}$

value is slightly bigger than $R_c^{(o)}$ for G_t>0.5. However, steady rolls are in a position to be competitive to other types of rolls, which may have small value of R_{20} >0, for the value of G_t >0.5 but very close to 0.5. A replacement for the figure 8 of R04 is Figure 14, which presents the transition boundary between subcritical and supercritical regimes for standing rolls-steady rolls in the (G_t, K_1)-plane with G=1.25 and three different values of K_2. The solution is supercritical in the region below the curve for given K_2 in figure 14, and subcritical above. The stabilizing effect of K_2 where the supercritical domain is enhanced by increasing the value of K_2, can be seen in this figure.

For the nonlinear problem due to the oscillatory rectangles-steady rectangles, our newly generated data for R_{20} for several different values of the angle γ provided results, which are given briefly as follows. The effect of K_1 is destabilizing in the sense that R_{20} decreases with increasing K_1. If K_1≥0.095, then most of the solutions in the form of standing rectangles-steady rectangles are subcritical. If K_1≥0.065, then most of the solutions in the form of general-travelling rectangles-steady rectangles are subcritical. A replacement for the figure 9 of R04 is Figure 15, which presents the transition boundary between subcritical and supercritical regimes for standing rectangles-steady rectangles in the (G_t, K_1)-plane with G=1.25, K_2=0.0.and for three different angles γ. Each of the solution is supercritical in the region below its transition curve and subcritical in the region above its transition curve. Hence, just below a transition curve for given G_t and K_1, the corresponding solution may have very small positive R_{20} and may well be preferred over the other solutions. A replacement for the figure 10 of R04 is Figure 16, which presents solid fraction versus z for a preferred supercritical solution in the form of standing rectangles-steady rectangles with γ=30°, G=1.25, G_t=0.5006, K_1=0.075 and K_2=0.0. It is seen from this figure there is tendency for chimney formation at an up-flow center or an up-flow vertex, and such tendency is higher in the lower-half of the layer. However, there is tendency for solid dendrite formation at a down-flow center or a down-flow vertex, and such tendency again is higher in the lower-half of the layer.

Our present study for the values of G_t and K_1 in the range 0.5001≤ G_t ≤0.534 and 0.0≤ K_1≤0.095 has detected many supercritical solutions with R_{10}=0 that can compete with one another in the sense that their corresponding R_{20} values can be very close to one another for given values of the parameters. However, for particular values of the parameters, it was possible to detect such solutions with the smallest possible values for their corresponding R_{20}. A replacement for the table 2 of R04 is the present Table 1, which presents new types of preferred supercritical mixed and simple (non-mixed) solutions, which correspond to the smallest value of R, for G=1.25, K_2=0 and for different values of G_t and K_1. In particular, as can be seen from the table 1 for a number of cases, supercritical solutions in the form of oscillatory hexagons can be the new types of the preferred solutions.

In regard to the stability of the finite-amplitude mixed solutions, the stability results for K_1≠0 are essentially those already given in R04. For K_1=0, no subcritical solution with R_{10}≠0 is possible and the only stable and preferred solution is that of simple-travelling rolls.

Finally, in section 5 of R04 the only two points that need to be updated are as follows. For an ammonium chloride-water solution of the kind used in the experimental studies by Tait et al. (1992), $G_t \approx 0.52$ can be relevant for a sufficiently thin layer. In the present investigation of the vertical distribution of the solid fraction due to the mixed solution in the form of standing hexagons-steady hexagons in the subcritical down-hexagonal state, we find tendency for the chimney formation at the cell nodes in whole depth of the mushy layer, which is in good agreement with the experimental results due to Tait et al. (1992)

6. Conclusion

We investigated the problem of nonlinear convection, due to oscillatory modes alone and also due to combined oscillatory and stationary modes, which are referred to as mixed modes, in horizontal mushy layers during the solidification of binary alloys. For the oscillatory problem, we carried out finite-amplitude and stability investigations for different values of the permeability parameters K_1 and K_2. We find that, depending on the values of the parameters, three-dimensional oscillatory solutions mostly in the form of simple-travelling rectangles or simple traveling hexagons can be the stable and preferred form of the flow solutions. Our results about the vertical distribution of solid fraction for the hexagonal solutions indicated possible beneficial effect of the oscillatory modes to reduce the tendency for chimney formation within the mushy layer.

For the mixed problem, we revisited the work of R04 and determined some new and updated results that are based on a more exact value of π, which involves in the numerical evaluation of the already determined analytical expressions in R04. For sufficiently small R or ε, the stable and preferred solution is found to be subcritical and composed of steady down-hexagonal mode and standing down-hexagonal mode. Depending on the values of the parameters, some new supercritical solutions, including oscillatory hexagons, were also predicted to be the preferred solutions for R beyond some value. The present investigation of the vertical distribution of solid fraction for this solution indicates that over the whole depth of the mushy layer, there are tendencies for the chimney formation at the cell's nodes and solid dendrite formation at the cell's center. The present results for such solution provide for the first time the best possible agreement of the analytical results based on a mathematical model with the available experimental observation for such flow problem.

Appendix

The system of equations and boundary conditions at order ε are given below

$\{\Delta_2(-\nabla^2 V_{10}+R_{00}\theta_{10}+R_{10}\theta_{00})=K_1\{\nabla^2(\phi_{00}\Delta_2 V_{00})+(\partial/\partial z)[(\partial^2 V_{00}/\partial x\partial z)(\partial\phi_{00}/\partial x)+(\partial^2 V_{00}$

$/\partial y\partial z)(\partial\phi_{00}/\partial y)+\pi^2 V_{00}(\partial\phi_{00}/\partial z)]$,

$\nabla^2\theta_{10}+G(R_{00}\Delta_2 V_{10}+R_{10}\Delta_2 V_{00}+R_{00}\mathbf{\Omega}V_{00}.\nabla\theta_{00})=0$,

$S[(\partial/\partial t_1)-(\partial/\partial z)]\phi_{10}+\nabla^2\theta_{10}+R_{00}\Delta_2 V_{10}= -R_{10}\Delta_2 V_{00}-(S\omega_{11}/\omega_{01})\partial\phi_{00}/\partial t_1+R_{00}\mathbf{\Omega}V_{00}.\nabla\theta_{00}$,

$V_{10}=\theta_{10}=0$ at $z=0$,

$V_{10}=\theta_{10}=\phi_{10}=0$ at $z=1$,

where $t_1=\omega t/\omega_{01}\}$. (A1)

The coefficient functions $B_{lp}^{(o)}$ and $E_{lp}^{(o)}$, which are introduced in (17a)-(17b), have the following expressions:

$(B_{lp}^{(o)}, E_{lp}^{(o)})=(B_{lp}^{(0)}, E_{lp}^{(0)})+(B_{lp}^{(1)}, E_{lp}^{(1)})\cos(2\pi z)+(B_{lp}^{(2)}, E_{lp}^{(2)})\sin(2\pi z)+(B_{lp}^{(3)}, E_{lp}^{(3)})$

$\cos(\pi z)exp[i\omega_{01}S_p(z-1)]+(B_{lp}^{(4)}, E_{lp}^{(4)})\sin(\pi z)exp[i\omega_{01}S_p(z-1)]$. (A2a)

Here

$(B_{lp}^{(0)}, E_{lp}^{(0)})=(1, a_{lp}^2\sqrt{G})C_1exp(r_{lp}^{(1)}z)+(1, a_{lp}^2\sqrt{G})C_2exp(-r_{lp}^{(1)}z)+(1, -a_{lp}^2\sqrt{G})C_3exp(r_{lp}^{(2)}$

$z)+(1, -a_{lp}^2\sqrt{G})C_4exp(-r_{lp}^{(2)}z)+(1, -GR_{00})L_{lp}^{(2)}$ for $\psi_{lp}\neq\pm1$, (A2b)

where

$\psi_{lp}=\boldsymbol{a}_l.\boldsymbol{a}_p/\pi^2$, $a_{lp}^2\equiv2\pi^2(1+\psi_{lp})$, $r_{lp}^{(1)}\equiv(a_{lp}^2+\sqrt{G}\,R_{00}\,a_{lp})^{0.5}$, $r_{lp}^{(2)}\equiv(a_{lp}^2-\sqrt{G}\,R_{00}\,a_{lp})^{0.5}$, $L_{lp}^{(2)}\equiv i$

$\omega_{01}K_1S_p\pi^3/[CG\sqrt{G}(\pi^2-\omega_{01}^2)(a_{lp}^2-GR_{00}^2)]$, $C_1\equiv[M_{lp}^{(1)}exp(-r_{lp}^{(1)})-M_{lp}^{(3)}]/[exp(r_{lp}^{(1)})-exp(-$

$r_{lp}^{(1)})]$, $C_2\equiv[M_{lp}^{(1)}exp(r_{lp}^{(1)})-M_{lp}^{(3)}]/[exp(r_{lp}^{(1)})-exp(-r_{lp}^{(1)})]$, $C_3\equiv[M_{lp}^{(2)}exp(-r_{lp}^{(2)})-M_{lp}^{(4)}]/[$

$exp(r_{lp}^{(2)})-exp(-r_{lp}^{(2)})]$, $C_4\equiv[M_{lp}^{(2)}exp(r_{lp}^{(2)})-M_{lp}^{(4)})]/[exp(r_{lp}^{(2)})-exp(-r_{lp}^{(2)})]$, $M_{lp}^{(1)}\equiv0.5[\sqrt{G}$

$R_{00}L_{lp}^{(2)}/a_{lp}^2-L_{lp}^{(2)}+L_{lp}^{(3)}+L_{lp}^{(4)}]$, $L_{lp}^{(3)}\equiv -B_{lp}^{(1)}-B_{lp}^{(3)}exp(-i\omega_{01}S_p)$, $L_{lp}^{(4)}\equiv[-E_{lp}^{(1)}-E_{lp}^{(3)}exp(-$

$i\omega_{01}S_p)]/a_{lp}^2$, $M_{lp}^{(2)}\equiv0.5[-\sqrt{G}\,R_{00}L_{lp}^{(2)}/a_{lp}^2-L_{lp}^{(2)}+L_{lp}^{(3)}-L_{lp}^{(4)}]$, $M_{lp}^{(3)}\equiv0.5[\sqrt{G}\,R_{00}L_{lp}^{(2)}/a_{lp}^2-$

$L_{lp}^{(2)}+L_{lp}^{(5)}+L_{lp}^{(6)}]$, $L_{lp}^{(5)}\equiv -B_{lp}^{(1)}+B_{lp}^{(3)}$, $L_{lp}^{(6)}\equiv(-E_{lp}^{(1)}+E_{lp}^{(3)})/a_{lp}^2$, $M_{lp}^{(4)}\equiv0.5[-\sqrt{G}\,R_{00}L_{lp}^{(2)}/$

$a_{lp}^2-L_{lp}^{(2)}+L_{lp}^{(5)}-L_{lp}^{(6)}]$; (A2c)

$B_{lp}^{(0)}=R_{00}[a_{lp}^2(L_{lp}^{(6)}-L_{lp}^{(4)})z^3/6+a_{lp}^2L_{lp}^{(4)}z^2/2]+L_{lp}^{(1)}z^2/2+\{-L_{lp}^{(3)}-0.5L_{lp}^{(1)}-R_{00}[a_{lp}^2(L_{lp}^{(6)}-L_{lp}^{(4)})/6+a_{lp}^2L_{lp}^{(4)}/2]+L_{lp}^{(5)}\}z+L_{lp}^{(3)}$ for $\psi_{lp}= -1$, $E_{lp}^{(0)}=a_{lp}^2(L_{lp}^{(6)}-L_{lp}^{(4)})z+a_{lp}^2L_{lp}^{(4)}$ for $\psi_{lp}= -1$, (A2d)

where

$L_{lp}^{(1)}\equiv -i\omega_{01}\pi^3S_pK_1/[CG\sqrt{G}(\pi^2-\omega_{01}^2)]$; (A2e)

$B_{lp}^{(0)}=C_5exp(r_{lp}^{(1)}z)+C_6exp(-r_{lp}^{(1)}z)+C_7z+C_8+0.25L_{lp}^{(1)}z$ for $\psi_{lp}=1$, $E_{lp}^{(0)}=2\pi\sqrt{G}[C_5 exp(r_{lp}^{(1)}z)+C_6exp(-r_{lp}^{(1)}z)-C_7z-C_8]-\sqrt{G}L_{lp}^{(1)}(0.5\pi z^2+0.25/\pi)$ for $\psi_{lp}=1$, (A2f)

where

$C_5\equiv[L_{lp}^{(8)}-L_{lp}^{(7)}exp(-r_{lp}^{(1)})]/[exp(r_{lp}^{(1)})-exp(-r_{lp}^{(1)})]$, $L_{lp}^{(7)}\equiv 0.5L_{lp}^{(3)}+L_{lp}^{(4)}a_{lp}^2/(4\pi\sqrt{G})+L_{lp}^{(1)}/(16\pi^2)$, $L_{lp}^{(8)}\equiv 0.5L_{lp}^{(5)}+L_{lp}^{(6)}a_{lp}^2/(4\pi\sqrt{G})-L_{lp}^{(1)}[1/8-\pi\sqrt{G}/4-\sqrt{G}/(8\pi)]$, $C_6\equiv[L_{lp}^{(7)}exp(r_{lp}^{(1)})-L_{lp}^{(8)}]/[exp(r_{lp}^{(1)})-exp(-r_{lp}^{(1)})]$, $C_7\equiv -C_5exp(r_{lp}^{(1)})-C_6exp(-r_{lp}^{(1)})-C_8-0.25L_{lp}^{(1)}+L_{lp}^{(5)}$, $C_8\equiv -L_{lp}^{(7)}+L_{lp}^{(3)}$; (A2g)

$B_{lp}^{(1)}=\{-2i\omega_{01}S_pK_1\pi^3/[CG\sqrt{G}(\pi^2-\omega_{01}^2)]\}/\{a_{lp}^2+4\pi^2-GR_{00}a_{lp}^2/(a_{lp}^2+4\pi^2)\}$, $E_{lp}^{(1)}= -GR_{00}a_{lp}^2B_{lp}^{(1)}/(a_{lp}^2+4\pi^2)$; (A2h)

$B_{lp}^{(2)}=\{\pi^2(1-\psi_{lp})-2K_1\pi^4(a_{lp}^2+4\pi^2)/[R_{00}CG\sqrt{G}(\pi^2-\omega_{01}^2)]\}/\{GR_{00}a_{lp}^2-(a_{lp}^2+4\pi^2)^2/R_{00}\}$,

$E_{lp}^{(2)}=2K_1\pi^4/[R_{00}CG\sqrt{G}(\pi^2-\omega_{01}^2)]-(a_{lp}^2+4\pi^2)B_{lp}^{(2)}/R_{00}$; (A2i)

$E_{lp}^{(3)}=E_{lp}^{(4)}=0$ for $\psi_{lp}= -1$, $B_{lp}^{(3)}= -i\omega_{01}S_pK_1\pi^3(\omega_{01}^2-5\pi^2)/[CG\sqrt{G}(\pi^2-\omega_{01}^2)^3]$ for $\psi_{lp}= -1$,

$B_{lp}^{(4)}=K_1\pi^4(3\pi^2+\omega_{01}^2)/[CG\sqrt{G}(\pi^2-\omega_{01}^2)^3]$ for $\psi_{lp}= -1$; (A2j)

$(E_{lp}^{(3)}, E_{lp}^{(4)})=[(C_9C_{13}-C_{11}C_{15}), (C_{10}C_{15}-C_9C_{12})]/(C_{10}C_{13}-C_{11}C_{12})$ for $\psi_{lp}\neq -1$, $(B_{lp}^{(3)}, B_{lp}^{(4)})=\{E_{lp}^{(3)}[(-a_{lp}^2-\pi^2-\omega_{01}^2), (-2i\omega_{01}S_p\pi)]+E_{lp}^{(4)}[(2i\omega_{01}S_p\pi), (-a_{lp}^2-\pi^2-\omega_{01}^2)]\}/(GR_{00}a_{lp}^2)$ for $\psi_{lp}\neq -1$, (A2k)

where

$C_9 \equiv i\omega_{01} S_p K_1 \pi^3 a_{lp}^2/[CG\sqrt{G}(\pi^2-\omega_{01}^2)]$, $C_{10} \equiv C_{13} \equiv -a_{lp}^2 R_{00}+[(a_{lp}^2+\pi^2+\omega_{01}^2)+4\omega_{01}^2\pi^2]/GR_{00}$,

$C_{11} \equiv -4i\omega_{01} S_p \pi(\pi^2+\omega_{01}^2+a_{lp}^2)/GR_{00} \equiv -C_{12}$, $C_{14} \equiv -3K_1\pi^4 a_{lp}^2/[CG\sqrt{G}(\pi^2-\omega_{01}^2)]$. (A2*l*)

The coefficient functions f_m^+, f_m^-, g_m^+, g_m^- and $f_{lp}^{(ij)}$ (i, j =0, 1, 2) , which are given in (17), have the following expressions:

$f_m^+ \equiv f_m = \{-2\pi^3\omega_{11}/[CG(\pi^2-\omega_{01}^2)^2]\}\{iS_m[(\pi^2+\omega_{01}^2)/\pi]\sin(\pi z)+2\omega_{01}\cos(\pi z)+[2\omega_{01}+iS_m(z-1)(\pi^2-\omega_{01}^2)]\exp[i\omega_{01}S_m(z-1)]\}$, $f_m^- = f_m^*$; (A3a)

$g_m^+ \equiv g_m = \{-R_{10}\pi/[C\sqrt{G}(\pi^2-\omega_{01}^2)]\}\{\pi\cos(\pi z)+i\omega_{01}S_m\sin(\pi z)+\pi\exp[i\omega_{01}S_m(z-1)]\}$, $g_m^- = g_m^*$; (A3b)

$f_{lp}^{(ij)} = -\langle H_{lp}^{(ij)}\exp(-h_{lp}^{(ij)}z)\rangle_1 \exp(-h_{lp}^{(ij)}z)+\langle H_{lp}^{(ij)}\exp(h_{lp}^{(ij)}z)\rangle_z \exp(-h_{lp}^{(ij)}z)$ (i, j=0, 1, 2), (A3c)

where

$\langle f\rangle_z \equiv \int_0^z f dz$, $\langle f\rangle_1 \equiv \int_0^1 f dz$, $(h_{lp}^{(00)}, H_{lp}^{(00)}) \equiv \{0, [R_{00}\, a_{lp}^2 B_{lp}^{(s)}-\pi^2\sin(2\pi z)(1-\psi_{lp})/G]/C\}$,

$(h_{lp}^{(10)}, H_{lp}^{(10)}) \equiv \{-i\omega_{01}S_l, H_{lp}^{(00)}\}$, $(h_{lp}^{(20)}, H_{lp}^{(20)}) \equiv \{i\omega_{01}S_l, H_{lp}^{(00)}\}$, $(h_{lp}^{(01)}, H_{lp}^{(01)}) \equiv \{-i\omega_{01}S_p,$

$[R_{00}\, a_{lp}^2 B_{lp}^{(o)}-\pi^2\sin(2\pi z)(1-\psi_{lp})/G]/C\}$, $(h_{lp}^{(02)}, H_{lp}^{(02)}) \equiv \{h_{lp}^{(01)*}, H_{lp}^{(01)*}\}$, $(h_{lp}^{(11)}, H_{lp}^{(11)}) \equiv \{-$

$i\omega_{01}(S_l+S_p), H_{lp}^{(01)}\}$, $(h_{lp}^{(12)}, H_{lp}^{(12)}) \equiv \{-i\omega_{01}(S_l-S_p), H_{lp}^{(01)*}\}$, $(h_{lp}^{(21)}, H_{lp}^{(21)}) \equiv \{h_{lp}^{(12)*}, H_{lp}^{(01)}$

$\}$, $(h_{lp}^{(22)}, H_{lp}^{(22)}) \equiv \{h_{lp}^{(11)*}, H_{lp}^{(01)*}\}$. (A3d)

The system of equations and boundary conditions at order ε^2 is

$\{\Delta_2(-\nabla^2 V_{20}+R_{00}\theta_{20}+R_{20}\theta_{00}) = \partial/\partial z[K_1(\mathbf{\Omega}V_{00}.\nabla\phi_{10}+\mathbf{\Omega}V_{10}.\nabla\phi_{00}) + K_2\,\mathbf{\Omega}V_{00}\,.\nabla(\phi_{00}^2)]+\nabla^2[\,K_1$

$(\phi_{10}\Delta_2 V_{00}+\phi_{00}\Delta_2 V_{10})+K_2\phi_{00}^2\Delta_2 V_{00}]$,

$\nabla^2\theta_{20}+G\Delta_2(R_{00}V_{20}+R_{20}V_{00}) = GR_{00}(\mathbf{\Omega}V_{00}.\nabla\theta_{10}+\mathbf{\Omega}V_{10}.\nabla\theta_{00})$,

$S(\partial/\partial t_1-\partial/\partial z)\phi_{20}+\Delta_2(R_{00}V_{20}+R_{20}V_{00})+\nabla^2\theta_{20} = -(S\omega_{21}/\omega_{01})(\partial/\partial t_1)\phi_{00}-(S\omega_{11}/\omega_{01})(\partial/\partial t_1)\phi_{10}+$

$R_{00}(\mathbf{\Omega}V_{00}.\nabla\theta_{10}+\mathbf{\Omega}V_{10}.\nabla\theta_{00})$,

$\theta_{20}=V_{20}=0$ at $z=0$, $\theta_{20}=V_{20}=\phi_{20}=0$ at $z=1\}$. (A4)

The solvability conditions for the system (A4) are reduced to the following equations:

$$R_{20}\sqrt{G}\pi(|A_n^+|^2+|A_n^-|^2)=\sum_{l,p,m}\{[E_{lpm}^{(1)}(A_n^+A_m^+A_l^+A_p^+<\eta_n^+\eta_m^+\eta_l^+\eta_p^+>+A_n^-A_m^+A_l^+A_p^+<\eta_n^-\eta_m^+\eta_l^+\eta_p^+>)+E_{lpm}^{(2)}(A_n^+A_m^-A_l^+A_p^+<\eta_n^+\eta_m^-\eta_l^+\eta_p^+>+A_n^-A_m^-A_l^+A_p^+<\eta_n^-\eta_m^-\eta_l^+\eta_p^+>)+E_{lpm}^{(3)}(A_n^+A_m^+A_l^+A_p^-<\eta_n^+\eta_m^+\eta_l^+\eta_p^->+A_n^-A_m^+A_l^+A_p^-<\eta_n^-\eta_m^+\eta_l^+\eta_p^->)+E_{lpm}^{(4)}(A_n^+A_m^-A_l^+A_p^-<\eta_n^+\eta_m^-\eta_l^+\eta_p^->+A_n^-A_m^-A_l^+A_p^-<\eta_n^-\eta_m^-\eta_l^+\eta_p^->)+E_{lpm}^{(5)}(A_n^+A_m^+A_l^-A_p^+<\eta_n^+\eta_m^+\eta_l^-\eta_p^+>+A_n^-A_m^+A_l^-A_p^+<\eta_n^-\eta_m^+\eta_l^-\eta_p^+>)+E_{lpm}^{(6)}(A_n^+A_m^-A_l^-A_p^+<\eta_n^+\eta_m^-\eta_l^-\eta_p^+>+A_n^-A_m^-A_l^-A_p^+<\eta_n^-\eta_m^-\eta_l^-\eta_p^+>)+E_{lpm}^{(7)}(A_n^+A_m^+A_l^-A_p^-<\eta_n^+\eta_m^+\eta_l^-\eta_p^->+A_n^-A_m^+A_l^-A_p^-<\eta_n^-\eta_m^+\eta_l^-\eta_p^->)+E_{lpm}^{(8)}(A_n^+A_m^-A_l^-A_p^-<\eta_n^+\eta_m^-\eta_l^-\eta_p^->+A_n^-A_m^-A_l^-A_p^-<\eta_n^-\eta_m^-\eta_l^-\eta_p^->)]\}, (n=-N, ...,-1, 1, ..., N). \quad (A5a)$$

Here the coefficient $E_{lpm}^{(i)}$(i=1, ..., 8) given in (A5a) have the following expressions:

$$E_{lpm}^{(1)}=K_1\pi^2(\psi_{ml}+\psi_{mp})<\cos^2(\pi z)f_{lp}^{(11)}>-0.5K_1\pi<\sin(2\pi z)(df_{lp}^{(11)}/dz)>+K_1\sqrt{G}\pi^2(\psi_{ml}+\psi_{mp})<\cos(\pi z)B_{lp}^{(o)}f_m>-K_1\sqrt{G}\,a_{lp}^2<\cos(\pi z)B_{lp}^{(o)}(df_m/dz)>+2K_2\pi^2\psi_{lp}<\cos^2(\pi z)f_mf_p>-K_2\pi<\sin(2\pi z)f_m(df_p/dz)>-K_1<\sin(\pi z)(d^2/dz^2-a_{lpm}^2)[\sin(\pi z)f_{lp}^{(11)}]>-(K_1\sqrt{G}/\pi)<\sin(\pi z)(d^2/dz^2-a_{lpm}^2)(B_{lp}^{(o)}f_m)>-K_2<\sin(\pi z)(d^2/dz^2-a_{lpm}^2)[\sin(\pi z)f_lf_p]>+0.5\sqrt{G}\pi^2R_{00}(\psi_{ml}+\psi_{mp})<\sin(2\pi z)E_{lp}^{(o)}>-\sqrt{G}\,\pi R_{00}<\sin^2(\pi z)(dE_{lp}^{(o)}/dz)>-GR_{00}\,\pi^2(\psi_{ml}+\psi_{mp})<\sin^2(\pi z)(dB_{lp}^{(o)}/dz)>+0.5GR_{00}\,\pi a_{lp}^2<\sin(2\pi z)B_{lp}^{(o)}>,\ a_{lpm}^2\equiv 2\pi^2(1.5+\psi_{lp}+\psi_{lm}+\psi_{pm}); \quad (A5b)$$

the expression for $E_{lpm}^{(2)}$ has the same form as the one given in (A9c), provided f_m is replaced by f_m^*; the expression for $E_{lpm}^{(3)}$ has the same form as the one given in (A9c), provided $f_{lp}^{(11)}$, $B_{lp}^{(o)}$, $E_{lp}^{(o)}$ and f_p are replaced, respectively, by $f_{lp}^{(12)}$, $B_{lp}^{(o)*}$, $E_{lp}^{(o)*}$ and f_p^*; the expression for $E_{lpm}^{(4)}$ is the same as the one for $E_{lpm}^{(3)}$, provided f_m is replaced by f_m^*; the expression for $E_{lpm}^{(5)}$ is the same as the one for $E_{lpm}^{(1)}$, provided $f_{lp}^{(11)}$ and f_l are replaced, respectively by $f_{lp}^{(21)}$ and f_l^*; the expression for $E_{lpm}^{(6)}$ is the same as the one for $E_{lpm}^{(5)}$, provided f_m is replaced by f_m^*; the expression for $E_{lpm}^{(7)}$ is the same as the one for $E_{lpm}^{(5)}$, provided $f_{lp}^{(21)}$, $B_{lp}^{(o)}$, $E_{lp}^{(o)}$ and f_p are replaced, respectively, by $f_{lp}^{(22)}$, $B_{lp}^{(o)*}$, $E_{lp}^{(o)*}$ and f_p^*; the expression for $E_{lpm}^{(8)}$ is the same as the one for $E_{lpm}^{(7)}$, provided f_m is replaced by f_m^*.

The expressions for the coefficients $T_{nm}^{(oi)}$(i=1, ..., 8), which were introduced in (19a), are given below

$$T_{nm}^{(o1)}=E^{(1)}_{-m,-n,m}\,\delta_{nm}+(E^{(1)}_{-m,-n,m}+E^{(1)}_{-n,-m,m})\delta_{n,-m}+(E^{(1)}_{-m.-n,m}+E^{(1)}_{-n,-m,m}+E^{(1)}_{m,-m,-n})(1-\delta_{nm})$$

$$(1-\delta_{n,-m}), \tag{A6a}$$

$$T_{nm}^{(o2)}=E^{(2)}_{-m,-n,m}\,\delta_{nm}+(E^{(2)}_{-m,-n,m}+E^{(2)}_{-n,-m,m})\delta_{n,-m}+(E^{(2)}_{-m,-n,m}+E^{(2)}_{-n,-m,m}+E^{(5)}_{m,-m,-n})(1-\delta_{nm})$$

$$(1-\delta_{n,-m}), \tag{A6b}$$

$$T_{nm}^{(o3)}=E^{(3)}_{-m,-n,m}\,\delta_{nm}+(E^{(3)}_{-m,-n,m}+E^{(5)}_{-n,-m,m})\delta_{n,-m}+(E^{(3)}_{-m,-n,m}+E^{(5)}_{-n,-m,m}+E^{(2)}_{m,-m,-n})(1-\delta_{nm})$$

$$(1-\delta_{n,-m}), \tag{A6c}$$

$$T_{nm}^{(o4)}=E^{(4)}_{-m,-n,m}\,\delta_{nm}+(E^{(4)}_{-m,-n,m}+E^{(6)}_{-n,-m,m})\delta_{n,-m}+(E^{(4)}_{-m,-n,m}+E^{(6)}_{-n,-m,}+E^{(6)}_{m,-m,-n})(1-\delta_{nm})$$

$$(1-\delta_{n,-m}), \tag{A6d}$$

$$T_{nm}^{(o5)}=E^{(5)}_{-m,-n,m}\,\delta_{nm}+(E^{(5)}_{-m,-n,m}+E^{(3)}_{-n,-m,m})\delta_{n,-m}+(E^{(5)}_{-m,-n,m}+E^{(3)}_{-n,-m,m}+E^{(3)}_{m,-m,-n})(1-\delta_{nm})$$

$$(1-\delta_{n,-m}), \tag{A6e}$$

$$T_{nm}^{(o6)}=E^{(6)}_{-m,-n,m}\,\delta_{nm}+(E^{(6)}_{-m,-n,m}+E^{(4)}_{-n,-m,m})\delta_{n,-m}+(E^{(6)}_{-m,-n,m}+E^{(4)}_{-n,-m,m}+E^{(7)}_{m,-m,-n})(1-\delta_{nm})$$

$$(1-\delta_{n,-m}), \tag{A6f}$$

$$T_{nm}^{(o7)}=E^{(7)}_{-m,-n,m}\,\delta_{nm}+(E^{(7)}_{-m,-n,m}+E^{(7)}_{-n,-m,m})\delta_{n,-m}+(E^{(7)}_{-m,-n,m}+E^{(7)}_{-n,-m,m}+E^{(4)}_{m,-m,-n})(1-\delta_{nm})$$

$$(1-\delta_{n,-m}), \tag{A6g}$$

$$T_{nm}^{(o8)}=E^{(8)}_{-m,-n,m}\,\delta_{nm}+(E^{(8)}_{-m,-n,m}+E^{(8)}_{-n,-m,m})\delta_{n,-m}+(E^{(8)}_{-m,-n,m}+E^{(8)}_{-n,-m,m}+E^{(8)}_{m,-m,-n})(1-\delta_{nm})$$

$$(1-\delta_{n,-m}), \tag{A6h}$$

where

$$\delta_{nm}=1 \text{ for } n=m \text{ and } 0 \text{ for } n\neq m. \tag{A6i}$$

The stability system is given below

$$\nabla^2[\varepsilon\phi'(d/d\tilde{\phi})K(\tilde{\phi})\Delta_2 V+K(\tilde{\phi})\Delta_2 V']+(\partial/\partial z)\{\varepsilon\mathbf{\Omega}V.\nabla[\phi'(d/d\tilde{\phi})K(\tilde{\phi})]+\mathbf{\Omega}V'.\nabla K(\tilde{\phi})\}-R\Delta_2\theta'=0, \tag{A7a}$$

$$(\partial/\partial t+\sigma-\delta\partial/\partial z)(-\theta'+S\phi'/\delta)+R(d\theta_B/dz)\Delta_2 V'+\nabla^2\theta'=\varepsilon R(\mathbf{\Omega}V.\nabla\theta'+\mathbf{\Omega}V'.\nabla\theta), \tag{A7b}$$

$(\partial/\partial t+\sigma-\delta\partial/\partial z)[(-1+\phi_B)\theta'+\theta_B\phi' +\varepsilon\phi\theta'+\varepsilon\phi'\theta-C\phi'/\delta]+R(d\theta_B/dz)\Delta_2 V'=\varepsilon R(\boldsymbol{\Omega}V.\nabla\theta'+$

$\boldsymbol{\Omega}V'.\nabla\theta)$, (A7c)

$$V' = \theta' =0 \text{ at } z =0, \tag{A7d}$$

$$V'= \theta' =\phi' =0 \text{ at } z =1. \tag{A7e}$$

REFERENCES

AMBERG, G. AND HOMSY, G. M. 1993 Nonlinear analysis of buoyant convection in binary solidification with application to channel formation. J. Fluid Mech. **252**, 79-98.

ANDERSON, D. M. AND WORSTER, M. G. 1995 Weakly nonlinear analysis of convection in mushy layers during the solidification of binary alloys. J. Fluid Mech. **302**, 307-331.

ANDERSON, D. M. AND WORSTER, M. G. 1996 A new oscillatory instability in a mushy layer during the solidification of binary alloys. J. Fluid Mech. **307**, 245-267.

BUSSE, F. H. 1967 The stability of finite amplitude convection and its relation to an extremum principal. J. Fluid Mech. **30**, 625-649.

BUSSE, F. H. 1975 Patterns of convection in spherical shells. J. Fluid Mech. **72**, 67-85.

CHANDRASEKHAR, S. 1961 Hydrodynamic and Hydromagnetic Stability. Clarendon.

RIAHI, D. N. 1983 Nonlinear convection in a porous layer with finite conducting boundaries. J. Fluid Mech. **129**, 153-171.

RIAHI, D. N. 2002 On nonlinear convection in mushy layers. Part1. Oscillatory modes of convection. J. Fluid Mech. **467**, 331-359.

RIAHI, D. N. 2004 On nonlinear convection in mushy layers. Part 2. Mixed oscillatory and stationary modes of convection. J. Fluid Mech. **517**, 71-101.

TAIT, S., JAHRLING, K. AND JAUPART, C. 1992 The planform of compositional convection and chimney formation in a mushy layer. Nature **359**, 406-408.

	.000	.015	.025	.035	.045	.055	.065	.075	.085	.095
.5001	4(o)	4(o)	10(o)	10(o)	12(o)	3(.3o)	7_d(o)	9_d(.4o)	6(.1)	5(o)
.5006	4(o)	4(o)	12(.1o)	10(o)	12(.4)	7_d(o)	9_c(.4o)	9_b	5	5(o)
.501	4(o)	10(o)	10(o)	7_d(o)	7_d(o)	3(.3o)	9_c(.4o)	7_a(o)	5	5(o)
.502	4(o)	10(o)	7_b(o)	7_b(o)	9_b(.3o)	3(.3o)	9_c(.2o)	7_a(o)	6(.1)	5(o)
.504	4(o)	10(o)	10(o)	7_d	10(o)	3(.3o)	12(.4o)	7_a(o)	12(.2o)	5(o)
.505	4(o)	10(o)	10(o)	10(o)	10(o)	9_d(.3o)	9_c(.3o)	7_a(o)	6(.3o)	5(o)
.507	4(o)	10(o)	10(o)	10(o)	10(o)	12(.4o)	9_c(.3o)	4(o)	8_b(o)	5(o)
.509	4(o)	10(o)	7_d(o)	7_d(o)	10(o)	7_c(o)	11(o)	4(o)	8_b(o)	5(o)
.512	4(o)	10(o)	7_d(o)	10(o)	10(o)	2(o)	7_d(o)	9_b(.3o)	9_b(.3o)	8_a(o)
.515	4(o)	10(o)	10(o)	7_d	10(o)	7_d(o)	9_c(.1o)	9_d(.1o)	6(.4)	5(o)
.518	4(o)	1(o)	(o)	7_d	10(o)	7_d(o)	7_a	8_d(o)	6(.3o)	5(o)
.522	4(o)	10(o)	10(o)	9_d(.4)	7_c(o)	12(.3o)	7_b	8_d(o)	6(.3o)	5(o)
.525	4(o)	10(o)	10(o)	9_c(.3)	10(o)	12(.3o)	7_b	8_d(o)	3(.4o)	5(o)
.530	4(o)	10(o)	10(o)	10(o)	10(o)	7_b(o)	11(o)	4	8_a(o)	5(o)
.534	4(o)	4(o)	10(o)	10(o)	10(o)	7_a(o)	9_b(.3)	8_d(o)	2(o)	5(o)

Table 1. Preferred supercritical solutions for G=1.25, K_2=0 and different values of G_t and K_1. Here a simple (non-mixed) oscillatory solution is designated by '(o)', and the rest of the notations are the same as those used in R04 for mixed types of solution. The first column and the first row present, respectively, the values of G_t and K_1. The value of the parameter b for the general traveling component of a preferred solution is given in parentheses. The subscripts, a, b, c and d present, respectively, the angles γ=15°, 30°, 50° and 70°.

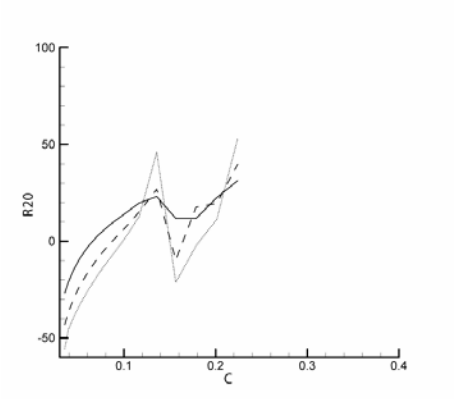

Figure 1. R_{20} versus C (S=0.25C) for the oscillatory solution in the form of simple-travelling hexagons. Here the graphs are for K_2=0 and for three different values of K_1=0.045 (solid line), 0.065 (dashed line) and 0.085 (dotted line).

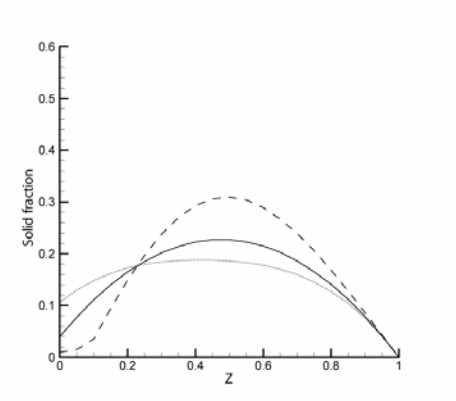

Figure 2. Solid fraction versus z for the oscillatory solution in the form of a preferred standing hexagons with ε=0.001, C=0.1565, S=0.25C, K_1=0.085 and K_2=0. Here the solid line, dashed line and dotted line present the basic solid fraction ϕ_B, $\phi(x=y=t=0)$ and $\phi(x=4/3, y=t=0)$, respectively.

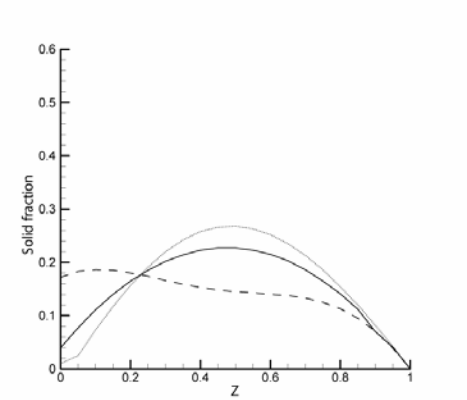

Figure 3. The same as the figure 2 but half period of oscillation later.

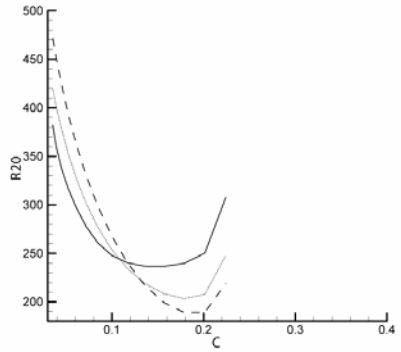

Figure 4. R_{20} versus C (S=0.25C) for the oscillatory solutions in the form of simple-travelling rolls (solid line), standing rolls (dashed line) and general-travelling rolls with b=0.3 (dotted line). The graphs are for K_1=0.065 and K_2=0.05.

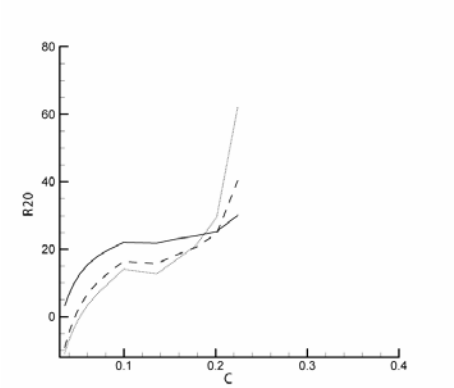

Figure 5. R_{20} versus C (S=0.25C) for the oscillatory solution in the form of simple-travelling squares for K_2=0 and three values of K_1=0.025 (solid line), 0.045 (dashed line) and 0.065 (dotted line).

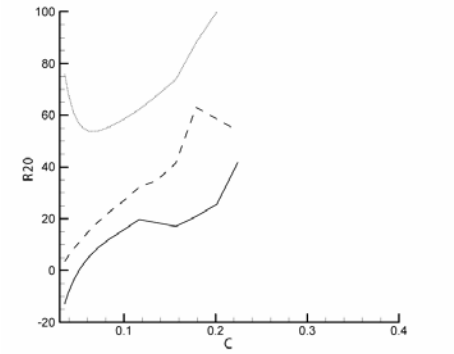

Figure 6. R_{20} versus C (S=0.25C) for the oscillatory solutions in the form of simple-travelling rectangles with three values of the angle γ=70° (solid line), 30° (dashed line) and 15° (dotted line). The graphs are for K_1=0.045 and K_2=0.

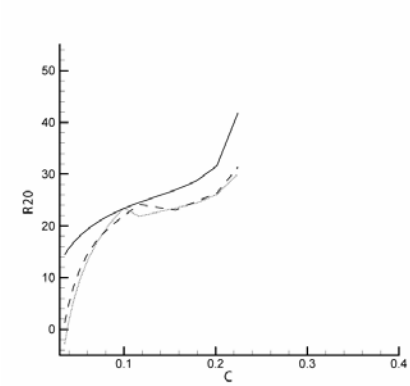

Figure 7. R_{20} versus C (S=0.25C) for the oscillatory solutions in the form of simple-travelling rolls (solid line), simple-travelling rectangles with γ=70° (dashed line) and simple-travelling hexagons (dotted line). The graphs are for K_1=0.025 and K_2=0.

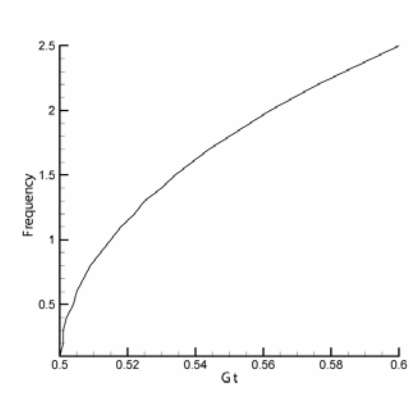

Figure 8. The frequency ω_{11} versus G_t.

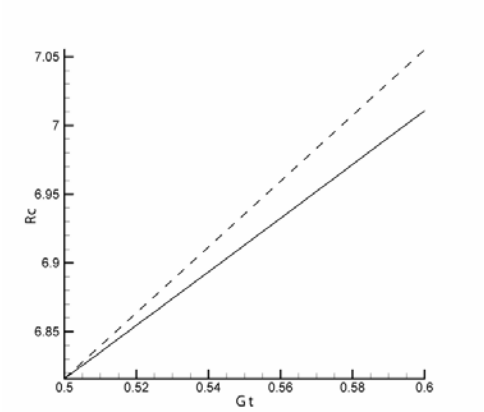

Figure 9. The critical values of the scaled Rayleigh number $R_c^{(o)}$ (solid line) and $R_c^{(s)}$ (dashed line) versus for G=1.25, K_1=1.0 and δ=0.2.

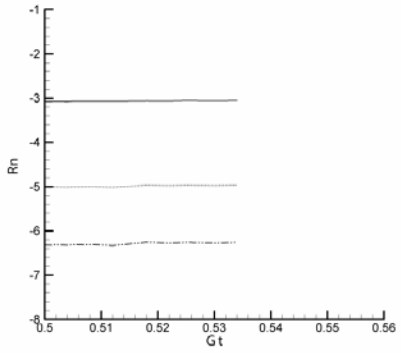

Figure 10. R_n versus G_t for subcritical flow in the form of subcritical standing down-hexagons-steady down-hexagons. Here the graphs are for G=1.25, K_2=0 and three values of K_1=0.0157 (solid line), 0.0251 (dotted line) and 0.0314 (dash-dot-dot line).

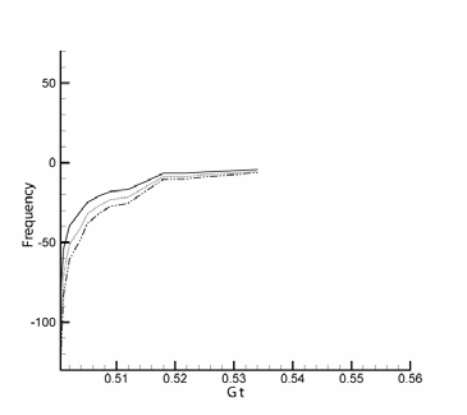

Figure 11. The same as in figure 10 but for ω_{11}.

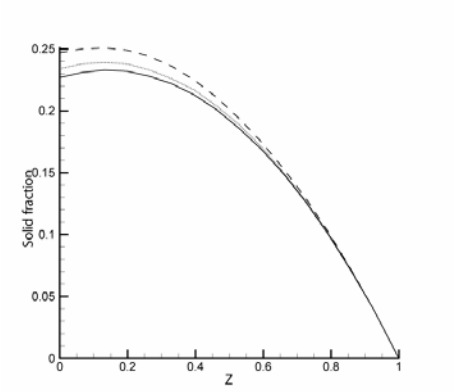

Figure 12. Solid fraction versus z for the preferred solution in the form of subcritical standing down-hexagons-steady down hexagons with ε=-0.001, G=1.25, G_t=0.502, K_1 =0.0157 and K_2=0. Here the dotted line, dashed line and solid line present the basic solid fraction ϕ_B, $\tilde{\phi}(x=y=0, t=0.5)$ and $\tilde{\phi}(x=4/3, y=0, t=0.5)$, respectively.

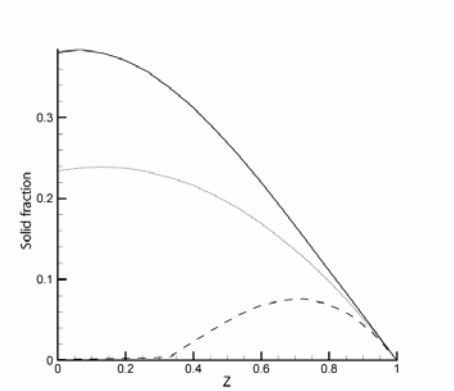

Figure 13. The same as in the figure 12 but for the up-hexagonal state (ε=0.001).

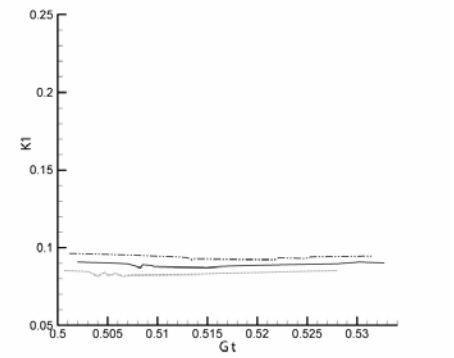

Figure 14. Transition boundary between subcritical and supercritical regimes for standing rolls-steady rolls in (G_t, K_1)-plane with G=1.25. Here dotted line, solid line and dash-dot-dot line present the cases of K_2=0.0, 0.001 and 0.002, respectively.

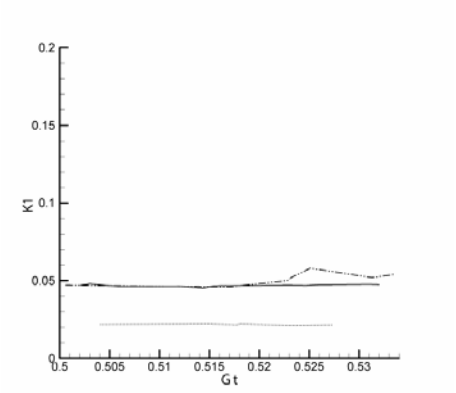

Figure 15. Transition boundary between subcritical and supercritical regimes for standing rectangles-steady rectangles in (G_t, K_1)-plane with G=1.25 and K_2=0. Here solid line, dotted line and dash-dot-dot line present the cases of γ=90° (squares), 56° and 50°, respectively.

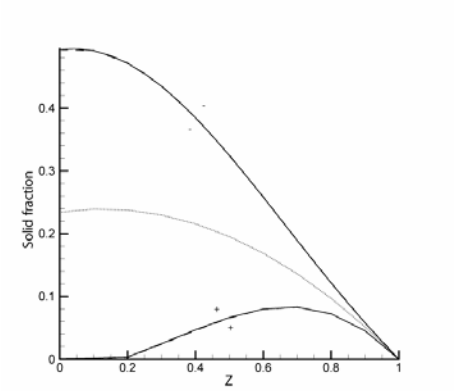

Figure 16. Solid fraction versus z for the solution in the form of standing rectangles-steady rectangles with γ=30°, G=1.25, G_t=0.5006, K_1=0.075 and K_2=0. Here dotted line, dashed line (±) and solid line (±) present the basic solid fraction ϕ_B, $\Phi(x= y = t=0, \varepsilon= \pm 0.001)$ and $\Phi(x=1.035, y=3.863, t=1.0, \varepsilon= \pm 0.001)$, respectively.

List of Recent TAM Reports

No.	*Authors*	*Title*	*Date*
996	Fried, E., and M. E. Gurtin	A nonequilibrium theory of epitaxial growth that accounts for surface stress and surface diffusion—*Journal of the Mechanics and Physics of Solids* **51**, 487–517 (2003)	Jan. 2002
997	Aref, H.	The development of chaotic advection—*Physics of Fluids* **14**, 1315–1325 (2002); see also *Virtual Journal of Nanoscale Science and Technology*, 11 March 2002	Jan. 2002
998	Christensen, K. T., and R. J. Adrian	The velocity and acceleration signatures of small-scale vortices in turbulent channel flow—*Journal of Turbulence*, in press (2002)	Jan. 2002
999	Riahi, D. N.	Flow instabilities in a horizontal dendrite layer rotating about an inclined axis—*Journal of Porous Media* **8**, 327–342 (2005)	Feb. 2002
1000	Kessler, M. R., and S. R. White	Cure kinetics of ring-opening metathesis polymerization of dicyclopentadiene—*Journal of Polymer Science A* **40**, 2373–2383 (2002)	Feb. 2002
1001	Dolbow, J. E., E. Fried, and A. Q. Shen	Point defects in nematic gels: The case for hedgehogs—*Archive for Rational Mechanics and Analysis* **177**, 21–51 (2005)	Feb. 2002
1002	Riahi, D. N.	Nonlinear steady convection in rotating mushy layers—*Journal of Fluid Mechanics* **485**, 279–306 (2003)	Mar. 2002
1003	Carlson, D. E., E. Fried, and S. Sellers	The totality of soft-states in a neo-classical nematic elastomer—*Journal of Elasticity* **69**, 169–180 (2003) with revised title	Mar. 2002
1004	Fried, E., and R. E. Todres	Normal-stress differences and the detection of disclinations in nematic elastomers—*Journal of Polymer Science B: Polymer Physics* **40**, 2098–2106 (2002)	June 2002
1005	Fried, E., and B. C. Roy	Gravity-induced segregation of cohesionless granular mixtures—*Lecture Notes in Mechanics*, in press (2002)	July 2002
1006	Tomkins, C. D., and R. J. Adrian	Spanwise structure and scale growth in turbulent boundary layers—*Journal of Fluid Mechanics* (submitted)	Aug. 2002
1007	Riahi, D. N.	On nonlinear convection in mushy layers: Part 2. Mixed oscillatory and stationary modes of convection—*Journal of Fluid Mechanics* **517**, 71–102 (2004)	Sept. 2002
1008	Aref, H., P. K. Newton, M. A. Stremler, T. Tokieda, and D. L. Vainchtein	Vortex crystals—*Advances in Applied Mathematics* **39**, in press (2002)	Oct. 2002
1009	Bagchi, P., and S. Balachandar	Effect of turbulence on the drag and lift of a particle—*Physics of Fluids*, in press (2003)	Oct. 2002
1010	Zhang, S., R. Panat, and K. J. Hsia	Influence of surface morphology on the adhesive strength of aluminum/epoxy interfaces—*Journal of Adhesion Science and Technology* **17**, 1685–1711 (2003)	Oct. 2002
1011	Carlson, D. E., E. Fried, and D. A. Tortorelli	On internal constraints in continuum mechanics—*Journal of Elasticity* **70**, 101–109 (2003)	Oct. 2002
1012	Boyland, P. L., M. A. Stremler, and H. Aref	Topological fluid mechanics of point vortex motions—*Physica D* **175**, 69–95 (2002)	Oct. 2002
1013	Bhattacharjee, P., and D. N. Riahi	Computational studies of the effect of rotation on convection during protein crystallization—*International Journal of Mathematical Sciences* **3**, 429–450 (2004)	Feb. 2003
1014	Brown, E. N., M. R. Kessler, N. R. Sottos, and S. R. White	*In situ* poly(urea-formaldehyde) microencapsulation of dicyclopentadiene—*Journal of Microencapsulation* (submitted)	Feb. 2003
1015	Brown, E. N., S. R. White, and N. R. Sottos	Microcapsule induced toughening in a self-healing polymer composite—*Journal of Materials Science* (submitted)	Feb. 2003
1016	Kuznetsov, I. R., and D. S. Stewart	Burning rate of energetic materials with thermal expansion—*Combustion and Flame* (submitted)	Mar. 2003

List of Recent TAM Reports (cont'd)

No.	*Authors*	*Title*	*Date*
1017	Dolbow, J., E. Fried, and H. Ji	Chemically induced swelling of hydrogels—*Journal of the Mechanics and Physics of Solids*, in press (2003)	Mar. 2003
1018	Costello, G. A.	Mechanics of wire rope—Mordica Lecture, Interwire 2003, Wire Association International, Atlanta, Georgia, May 12, 2003	Mar. 2003
1019	Wang, J., N. R. Sottos, and R. L. Weaver	Thin film adhesion measurement by laser induced stress waves—*Journal of the Mechanics and Physics of Solids* (submitted)	Apr. 2003
1020	Bhattacharjee, P., and D. N. Riahi	Effect of rotation on surface tension driven flow during protein crystallization—*Microgravity Science and Technology* **14**, 36–44 (2003)	Apr. 2003
1021	Fried, E.	The configurational and standard force balances are not always statements of a single law—*Proceedings of the Royal Society* (submitted)	Apr. 2003
1022	Panat, R. P., and K. J. Hsia	Experimental investigation of the bond coat rumpling instability under isothermal and cyclic thermal histories in thermal barrier systems—*Proceedings of the Royal Society of London A* **460**, 1957–1979 (2003)	May 2003
1023	Fried, E., and M. E. Gurtin	A unified treatment of evolving interfaces accounting for small deformations and atomic transport: grain-boundaries, phase transitions, epitaxy—*Advances in Applied Mechanics* **40**, 1–177 (2004)	May 2003
1024	Dong, F., D. N. Riahi, and A. T. Hsui	On similarity waves in compacting media—*Horizons in World Physics* **244**, 45–82 (2004)	May 2003
1025	Liu, M., and K. J. Hsia	Locking of electric field induced non-180° domain switching and phase transition in ferroelectric materials upon cyclic electric fatigue—*Applied Physics Letters* **83**, 3978–3980 (2003)	May 2003
1026	Liu, M., K. J. Hsia, and M. Sardela Jr.	In situ X-ray diffraction study of electric field induced domain switching and phase transition in PZT-5H—*Journal of the American Ceramics Society* (submitted)	May 2003
1027	Riahi, D. N.	On flow of binary alloys during crystal growth—*Recent Research Development in Crystal Growth* **3**, 49–59 (2003)	May 2003
1028	Riahi, D. N.	On fluid dynamics during crystallization—*Recent Research Development in Fluid Dynamics* **4**, 87–94 (2003)	July 2003
1029	Fried, E., V. Korchagin, and R. E. Todres	Biaxial disclinated states in nematic elastomers—*Journal of Chemical Physics* **119**, 13170–13179 (2003)	July 2003
1030	Sharp, K. V., and R. J. Adrian	Transition from laminar to turbulent flow in liquid filled microtubes—*Physics of Fluids* (submitted)	July 2003
1031	Yoon, H. S., D. F. Hill, S. Balachandar, R. J. Adrian, and M. Y. Ha	Reynolds number scaling of flow in a Rushton turbine stirred tank: Part I—Mean flow, circular jet and tip vortex scaling—*Chemical Engineering Science* (submitted)	Aug. 2003
1032	Raju, R., S. Balachandar, D. F. Hill, and R. J. Adrian	Reynolds number scaling of flow in a Rushton turbine stirred tank: Part II—Eigen-decomposition of fluctuation—*Chemical Engineering Science* (submitted)	Aug. 2003
1033	Hill, K. M., G. Gioia, and V. V. Tota	Structure and kinematics in dense free-surface granular flow—*Physical Review Letters* **91**, 064302 (2003)	Aug. 2003
1034	Fried, E., and S. Sellers	Free-energy density functions for nematic elastomers—*Journal of the Mechanics and Physics of Solids* **52**, 1671–1689 (2004)	Sept. 2003
1035	Kasimov, A. R., and D. S. Stewart	On the dynamics of self-sustained one-dimensional detonations: A numerical study in the shock-attached frame—*Physics of Fluids* (submitted)	Nov. 2003
1036	Fried, E., and B. C. Roy	Disclinations in a homogeneously deformed nematic elastomer—*Nature Materials* (submitted)	Nov. 2003
1037	Fried, E., and M. E. Gurtin	The unifying nature of the configurational force balance—*Mechanics of Material Forces* (P. Steinmann and G. A. Maugin, eds.), in press (2003)	Dec. 2003
1038	Panat, R., K. J. Hsia, and J. W. Oldham	Rumpling instability in thermal barrier systems under isothermal conditions in vacuum—*Philosophical Magazine*, in press (2004)	Dec. 2003

List of Recent TAM Reports (cont'd)

No.	Authors	Title	Date
1039	Cermelli, P., E. Fried, and M. E. Gurtin	Sharp-interface nematic–isotropic phase transitions without flow—*Archive for Rational Mechanics and Analysis* **174**, 151–178 (2004)	Dec. 2003
1040	Yoo, S., and D. S. Stewart	A hybrid level-set method in two and three dimensions for modeling detonation and combustion problems in complex geometries—*Combustion Theory and Modeling* (submitted)	Feb. 2004
1041	Dienberg, C. E., S. E. Ott-Monsivais, J. L. Ranchero, A. A. Rzeszutko, and C. L. Winter	Proceedings of the Fifth Annual Research Conference in Mechanics (April 2003), TAM Department, UIUC (E. N. Brown, ed.)	Feb. 2004
1042	Kasimov, A. R., and D. S. Stewart	Asymptotic theory of ignition and failure of self-sustained detonations—*Journal of Fluid Mechanics* (submitted)	Feb. 2004
1043	Kasimov, A. R., and D. S. Stewart	Theory of direct initiation of gaseous detonations and comparison with experiment—*Proceedings of the Combustion Institute* (submitted)	Mar. 2004
1044	Panat, R., K. J. Hsia, and D. G. Cahill	Evolution of surface waviness in thin films via volume and surface diffusion—*Journal of Applied Physics* (submitted)	Mar. 2004
1045	Riahi, D. N.	Steady and oscillatory flow in a mushy layer—*Current Topics in Crystal Growth Research*, in press (2004)	Mar. 2004
1046	Riahi, D. N.	Modeling flows in protein crystal growth—*Current Topics in Crystal Growth Research*, in press (2004)	Mar. 2004
1047	Bagchi, P., and S. Balachandar	Response of the wake of an isolated particle to isotropic turbulent cross-flow—*Journal of Fluid Mechanics* (submitted)	Mar. 2004
1048	Brown, E. N., S. R. White, and N. R. Sottos	Fatigue crack propagation in microcapsule toughened epoxy—*Journal of Materials Science* (submitted)	Apr. 2004
1049	Zeng, L., S. Balachandar, and P. Fischer	Wall-induced forces on a rigid sphere at finite Reynolds number—*Journal of Fluid Mechanics* (submitted)	May 2004
1050	Dolbow, J., E. Fried, and H. Ji	A numerical strategy for investigating the kinetic response of stimulus-responsive hydrogels—*Computer Methods in Applied Mechanics and Engineering* **194**, 4447–4480 (2005)	June 2004
1051	Riahi, D. N.	Effect of permeability on steady flow in a dendrite layer—*Journal of Porous Media*, in press (2004)	July 2004
1052	Cermelli, P., E. Fried, and M. E. Gurtin	Transport relations for surface integrals arising in the formulation of balance laws for evolving fluid interfaces—*Journal of Fluid Mechanics* (submitted)	Sept. 2004
1053	Stewart, D. S., and A. R. Kasimov	Theory of detonation with an embedded sonic locus—*SIAM Journal on Applied Mathematics* (submitted)	Oct. 2004
1054	Stewart, D. S., K. C. Tang, S. Yoo, M. Q. Brewster, and I. R. Kuznetsov	Multi-scale modeling of solid rocket motors: Time integration methods from computational aerodynamics applied to stable quasi-steady motor burning—*Proceedings of the 43rd AIAA Aerospace Sciences Meeting and Exhibit* (January 2005), Paper AIAA-2005-0357 (2005)	Oct. 2004
1055	Ji, H., H. Mourad, E. Fried, and J. Dolbow	Kinetics of thermally induced swelling of hydrogels—*International Journal of Solids and Structures* (submitted)	Dec. 2004
1056	Fulton, J. M., S. Hussain, J. H. Lai, M. E. Ly, S. A. McGough, G. M. Miller, R. Oats, L. A. Shipton, P. K. Shreeman, D. S. Widrevitz, and E. A. Zimmermann	Final reports: Mechanics of complex materials, Summer 2004 (K. M. Hill and J. W. Phillips, eds.)	Dec. 2004
1057	Hill, K. M., G. Gioia, and D. R. Amaravadi	Radial segregation patterns in rotating granular mixtures: Waviness selection—*Physical Review Letters* **93**, 224301 (2004)	Dec. 2004

List of Recent TAM Reports (cont'd)

No.	*Authors*	*Title*	*Date*
1058	Riahi, D. N.	Nonlinear oscillatory convection in rotating mushy layers—*Journal of Fluid Mechanics*, in press (2005)	Dec. 2004
1059	Okhuysen, B. S., and D. N. Riahi	On buoyant convection in binary solidification—*Journal of Fluid Mechanics* (submitted)	Jan. 2005
1060	Brown, E. N., S. R. White, and N. R. Sottos	Retardation and repair of fatigue cracks in a microcapsule toughened epoxy composite—Part I: Manual infiltration—*Composites Science and Technology* (submitted)	Jan. 2005
1061	Brown, E. N., S. R. White, and N. R. Sottos	Retardation and repair of fatigue cracks in a microcapsule toughened epoxy composite—Part II: *In situ* self-healing—*Composites Science and Technology* (submitted)	Jan. 2005
1062	Berfield, T. A., R. J. Ong, D. A. Payne, and N. R. Sottos	Residual stress effects on piezoelectric response of sol-gel derived PZT thin films—*Journal of Applied Physics* (submitted)	Apr. 2005
1063	Anderson, D. M., P. Cermelli, E. Fried, M. E. Gurtin, and G. B. McFadden	General dynamical sharp-interface conditions for phase transformations in viscous heat-conducting fluids—*Journal of Fluid Mechanics* (submitted)	Apr. 2005
1064	Fried, E., and M. E. Gurtin	Second-gradient fluids: A theory for incompressible flows at small length scales—*Journal of Fluid Mechanics* (submitted)	Apr. 2005
1065	Gioia, G., and F. A. Bombardelli	Localized turbulent flows on scouring granular beds—*Physical Review Letters*, in press (2005)	May 2005
1066	Fried, E., and S. Sellers	Orientational order and finite strain in nematic elastomers—*Journal of Chemical Physics* **123**, 044901 (2005)	May 2005
1067	Chen, Y.-C., and E. Fried	Uniaxial nematic elastomers: Constitutive framework and a simple application—*Proceedings of the Royal Society of London A*, in press (2005)	June 2005
1068	Fried, E., and S. Sellers	Incompatible strains associated with defects in nematic elastomers—*Journal of Chemical Physics*, in press (2005)	Aug. 2005
1069	Gioia, G., and X. Dai	Surface stress and reversing size effect in the initial yielding of ultrathin films—*Journal of Applied Mechanics*, in press (2005)	Aug. 2005
1070	Gioia, G., and P. Chakraborty	Turbulent friction in rough pipes and the energy spectrum of the phenomenological theory—*arXiv:physics* 0507066 v1 8 Jul 2005	Aug. 2005
1071	Keller, M. W., and N. R. Sottos	Mechanical properties of capsules used in a self-healing polymer—*Experimental Mechanics* (submitted)	Sept. 2005
1072	Chakraborty, P., G. Gioia, and S. Kieffer	Volcán Reventador's unusual umbrella	Sept. 2005
1073	Fried, E., and S. Sellers	Soft elasticity is not necessary for striping in nematic elastomers—*Nature Physics* (submitted)	Sept. 2005
1074	Fried, E., M. E. Gurtin, and Amy Q. Shen	Theory for solvent, momentum, and energy transfer between a surfactant solution and a vapor atmosphere—*Physical Review E* (submitted)	Sept. 2005
1075	Chen, X., and E. Fried	Rayleigh–Taylor problem for a liquid–liquid phase interface—*Journal of Fluid Mechanics* (submitted)	Oct. 2005
1076	Riahi, D. N.	Mathematical modeling of wind forces—In *The Euler Volume* (Abington, UK: Taylor and Francis), in press (2005)	Oct. 2005
1077	Fried, E., and R. E. Todres	Mind the gap: The shape of the free surface of a rubber-like material in the proximity to a rigid contactor—*Journal of Elasticity*, in press (2006)	Oct. 2005
1078	Riahi, D. N.	Nonlinear compositional convection in mushy layers—*Journal of Fluid Mechanics* (submitted)	Dec. 2005